UNCLASSIFIED

AD 282 808

Reproduced
by the

ARMED SERVICES TECHNICAL INFORMATION AGENCY
ARLINGTON HALL STATION
ARLINGTON 12, VIRGINIA

19990921103

UNCLASSIFIED

DEPARTMENT OF ELECTRICAL ENGINEERING

UNIVERSITY OF UTAH

SALT LAKE CITY, UTAH

282 808

HYPER-ELASTIC IMPACTS

Neil P. Bailey, C. Eugene McDermott,
Dietrich K. Gehmlich, E. P. Palmer

Technical Report UU-8
1 May 1962

High Velocity Laboratory
Department of Electrical Engineering
University of Utah
Salt Lake City, Utah

TABLE OF CONTENTS

SYMBOLS USED AND UNITS IN EQUATIONS

c -- a dimensionless energy ratio of materials

e -- unit compressive deformation, ft. per ft.

E -- compressive modulus of elasticity, lb. per sq. ft.

f -- stressing turbulence factor, dimensionless

H -- length, ft.

S -- unit compressive stress, lb. per sq. ft.

t -- time, sec.

u -- internal energy, ft. lb. per cu.ft.

V -- material velocity, ft. per sec.

W -- wave velocity, ft. per sec.

x -- distance, ft.

ρ -- material density, slugs per cu. ft.

HYPER-ELASTIC IMPACTS

1. THEORY AND ANALYSIS

1.1 Introduction

During the high-velocity impacts of metal objects, stresses beyond the elastic range of the materials are developed and waves which will be designated "hyper-elastic waves" are propagated. It is the purpose of this report to investigate such one-dimensional hyper-elastic waves in metal rods that are impacted in and above the elastic range.

1.2 The Nature of Hyper-Elastic Waves

It seems to be currently popular to attempt the explanation of hyper-elastic waves by contriving an equivalent bulk elasticity for metals and treating such explosion or impact produced disturbances as classical fluid waves. Such an over-simplified approach fails to explain some of the most important and easily observable facts of such a disturbance.

    a. It is not a single wave passing through the material since the metal near the impacted end of a bar is permanently deformed and "up-set" when the metal further from the end is relatively unharmed.

    b. A strain gage record of the disturbance as it progresses along a bar shows it not to be a classical square wave front. Instead, it is a front of decreasing steepness with definite evidence of inelastic slip.

    c. The discontinuous and non-linear nature of the stress-strain curve of a metal does not suggest that its load-deformation nature and action can be described by a single number.

It therefore seems much more logical to base the analysis of such disturbances on the observed stress-strain nature of actual metals rather than to treat them as fluids with continuous properties.

1.3 The Elastic Recovery of Metals

The obvious physical properties of metals are summed up by their stress S deformation e curves which characteristically have a linear portion followed by a non-linear section terminating at the ultimate stress. The ultimate stress in compression is clearly defined for brittle materials but not always so evident for ductile metals. The linear portion seems not to be altered by the rate of loading, but the non-linear portion can be changed slightly by the rate of loading during testing, particularly at higher strains.

The non-linear portion is referred to as inelastic and the linear portion as the elastic range. That this linear range is not truly elastic in the reversible sense is made quite evident by the observed fact that for cyclic stresses in this so-called elastic range internal hysteresis losses of considerable magnitude can be measured.

Another indication that this linear and so-called elastic portion of the stress-strain curve does not reveal all that goes on occurs when elastic waves are propagated in metal bars. For a metal having an elastic modulus $E_2 = \frac{S}{e}$ and a mass density ρ, such waves should propagate at a velocity $\sqrt{\frac{E_2}{\rho}}$. However, careful tests consistently result in propagation velocities greater than this.

The stress-strain curve depicted by Fig. 1.1 reflects only the input work required to deform the material and as such is incapable of revealing what became of this input deforming work. One certain way of determining
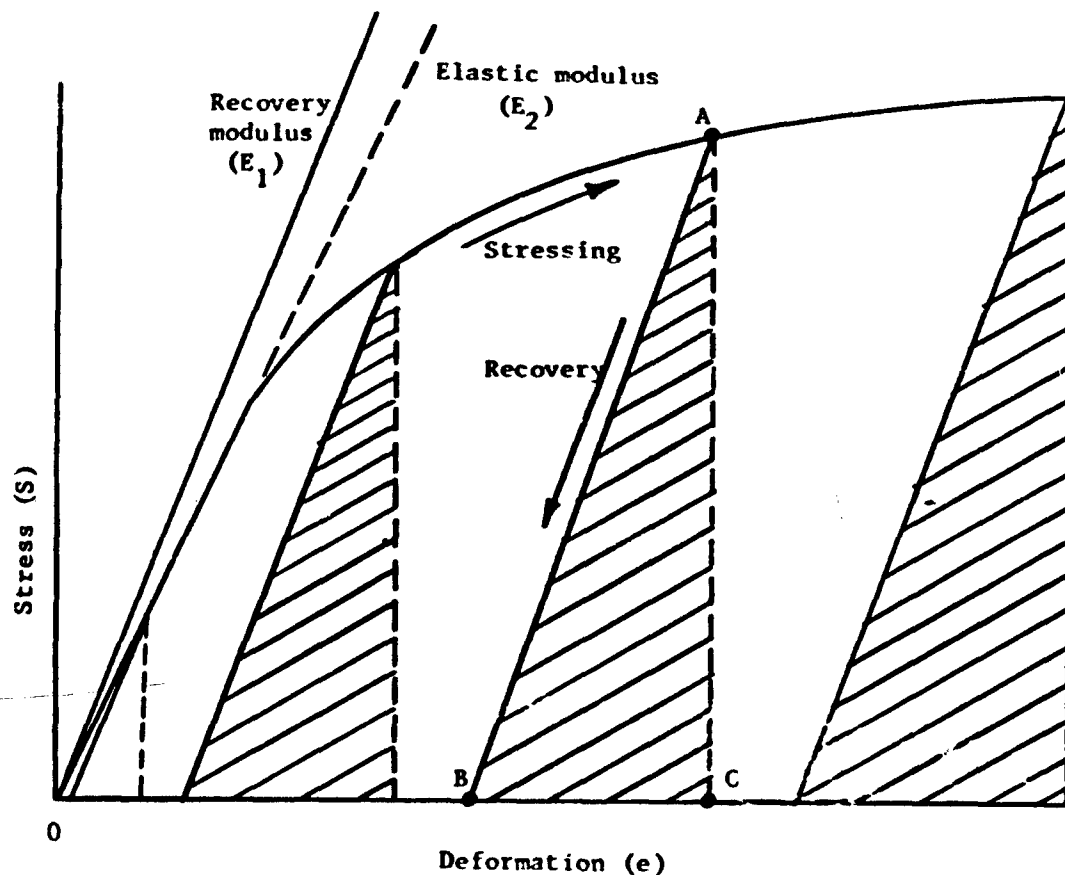
Fig. 1.1

the portion of this input energy that is stored elastically is to ask the

stressed material how much energy it can return when the stress is released.

This returnable energy is, by definition, the reversible, elastically

stored energy.

This is accomplished experimentally by stressing the metal to condition A,

Fig. 1.1, and then determining the recovery line A-B as the stress is released.

If this is done at various stresses up to the ultimate, each time on a

fresh specimen, two things become apparent. The recovery lines A-B are

straight lines and all of the recovery triangles A-B-C are similar triangles.

If in each case the recovery energy is expressed as $u = \dfrac{eS}{2}$ or $\dfrac{S^2}{2E_1}$, the

recovery modulus E_1 so calculated gives the recovery curve with slope E_1

- 3 -

as illustrated by Fig. 1.1. Figures 1.2, 1.3, and 1.4 show such test results for steel, alumirum, and copper. One significance of the recovery modulus E_1 is illustrated by Table 1.1.

Metal	ρ Slugs per Cu.Ft.	E_1 psi	E_2 psi	$\sqrt{E_1/\rho}$ ft.per sec.	$\sqrt{E_2/\rho}$	Test Velocity
Steel	15.15	35,900,000	29,300,000	18,500	16,700	18,400
Aluminum	5.36	12,400,000	10,600,000	18,200	16,800	17,900
Copper	17.28	19,800,000	16,000,000	12,700	11,540	13,400

TABLE 1.1

As is shown by Table 1.1, the propagation velocity calculated from the recovery modulus E_1 comes much closer to checking with the test velocity of disturbances than does the value $\sqrt{E_2/\rho}$ calculated from the conventional elastic modulus.

1.4 Generalized Stress-Strain Curves

Before undertaking the analysis of hyper-elastic waves, it is helpful to look at the effect of the stress-strain curve shape on the propagation of waves in materials. It was first shown for concrete by Talbot[1] and later for other materials by Gilkey and Murphy[2] that quite different appearing stress-strain curves can be reduced to essentially similar curves for each class materials by making a unit or dimensionless plot of S/S_u vs e/e_u where S is unit stress and e is unit strain. Correspondingly, S_u and e_u

---

[1] Talbot, A. N., "Tests of Reinforced Concrete Beams, Series of 1905," Bul. 4, Eng. Ex. Station, University of Illinois, Urbana, 1906.

[2] H. J. Gilkey and Glenn Murphy, "The Percentage Stress-Strain Diagram as an Index to the Comparative Behavior of Materials Under Load," Iowa Engineering Bulletin 159, Iowa State College, Ames, 1943.

- 4 -

UNIT STRAIN e $(10^{-3}$ in/in)

$E_1 = 35.9 \times 10^6$ psi

$E_1 = 35.9 \times 10^6$ psi →

$E_2 = 29.3 \times 10^6$ psi (elastic)

$E_1 = 35.9 \times 10^6$ psi

Superimposed energy triangles

UNIT STRESS S$(10^3$ psi)

Fig. 1.2. Unit stress plotted against unit strain for 1018 steel in compression. Specimens of 3/4" diameter and 2" long were used.

UNIT STRAIN e (10^{-3} in/in)

STRAIN ENERGY / UNIT STRESS X UNIT STRAIN ($\frac{U}{Se}$)

Fig. 1.2a. Strain energy divided by unit stress times unit strain ($\frac{U}{Se}$) plotted against unit strain (e) for 1018 steel in compression. Specimens of 3/4" diameter and 2" long were used.

- 6 -
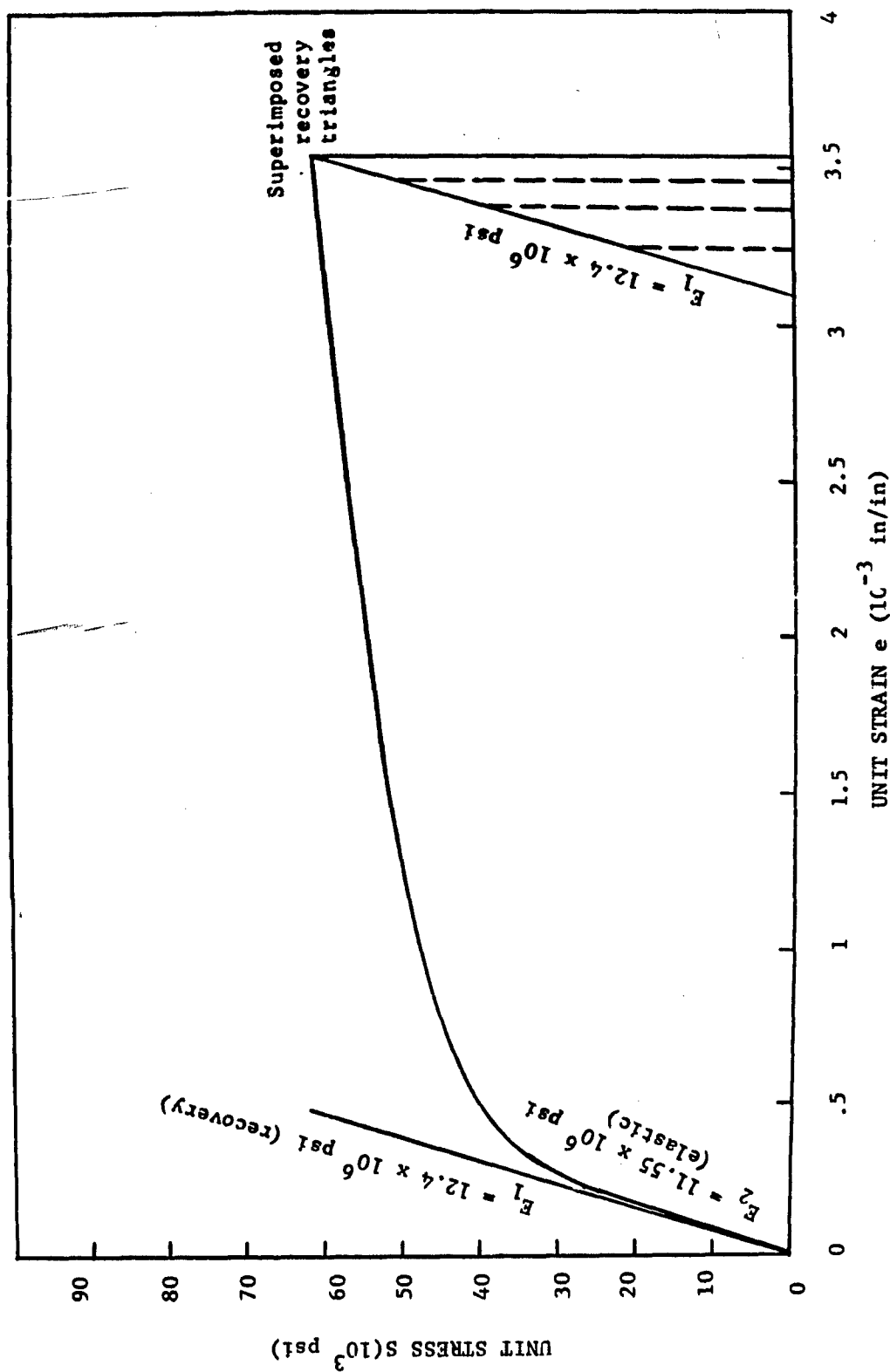
Fig. 1.3. Unit stress plotted against unit strain for 24T4 aluminum in compression. Specimens of 3/4" diameter and 2" long were used.

Fig. 1.3a. Strain energy divided by the unit stress times unit strain ($\frac{U}{Se}$) plotted against unit strain (e) 24T4 aluminum in compression. Specimens of 3/4" diameter and 2" long were used.
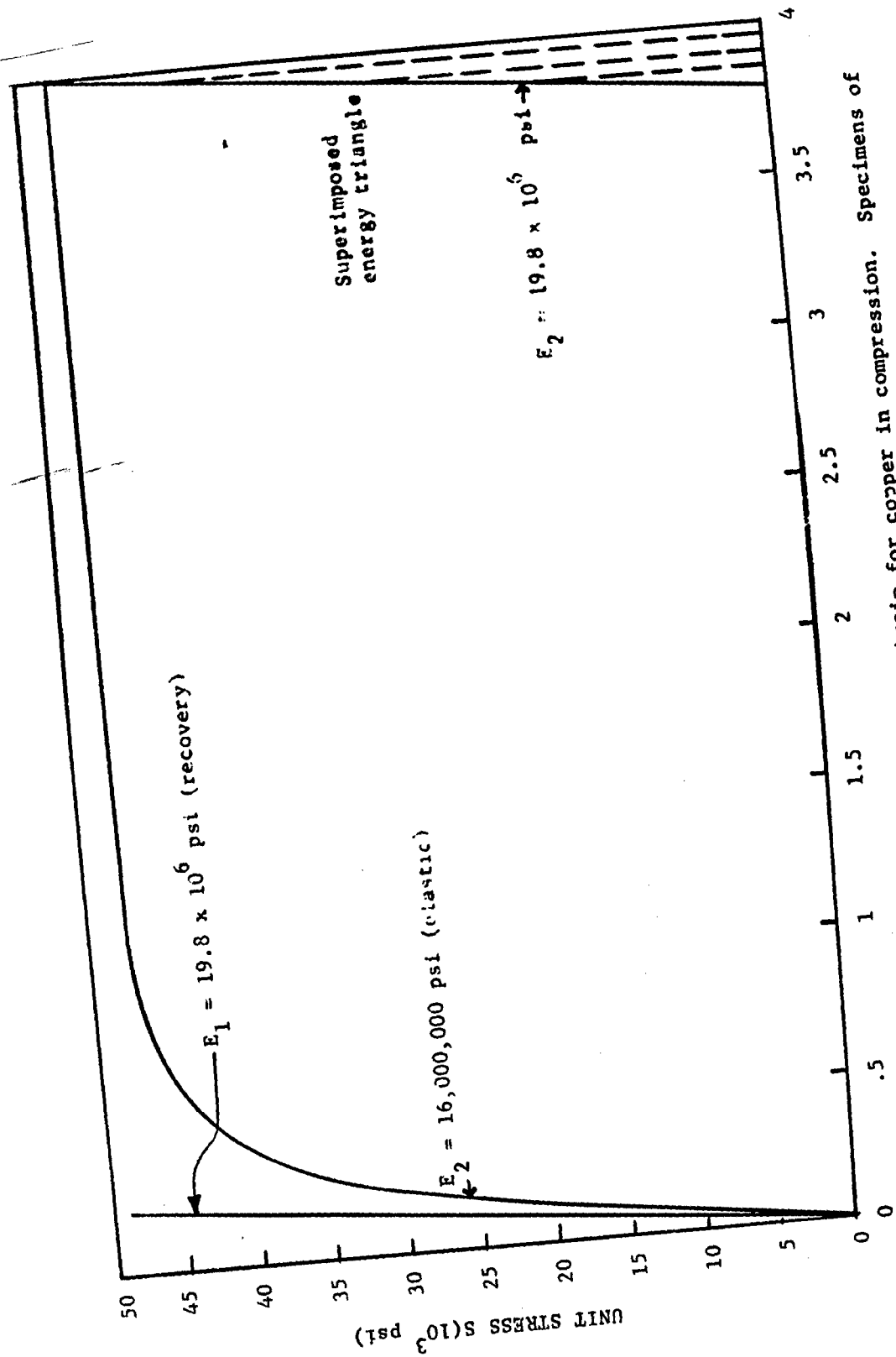
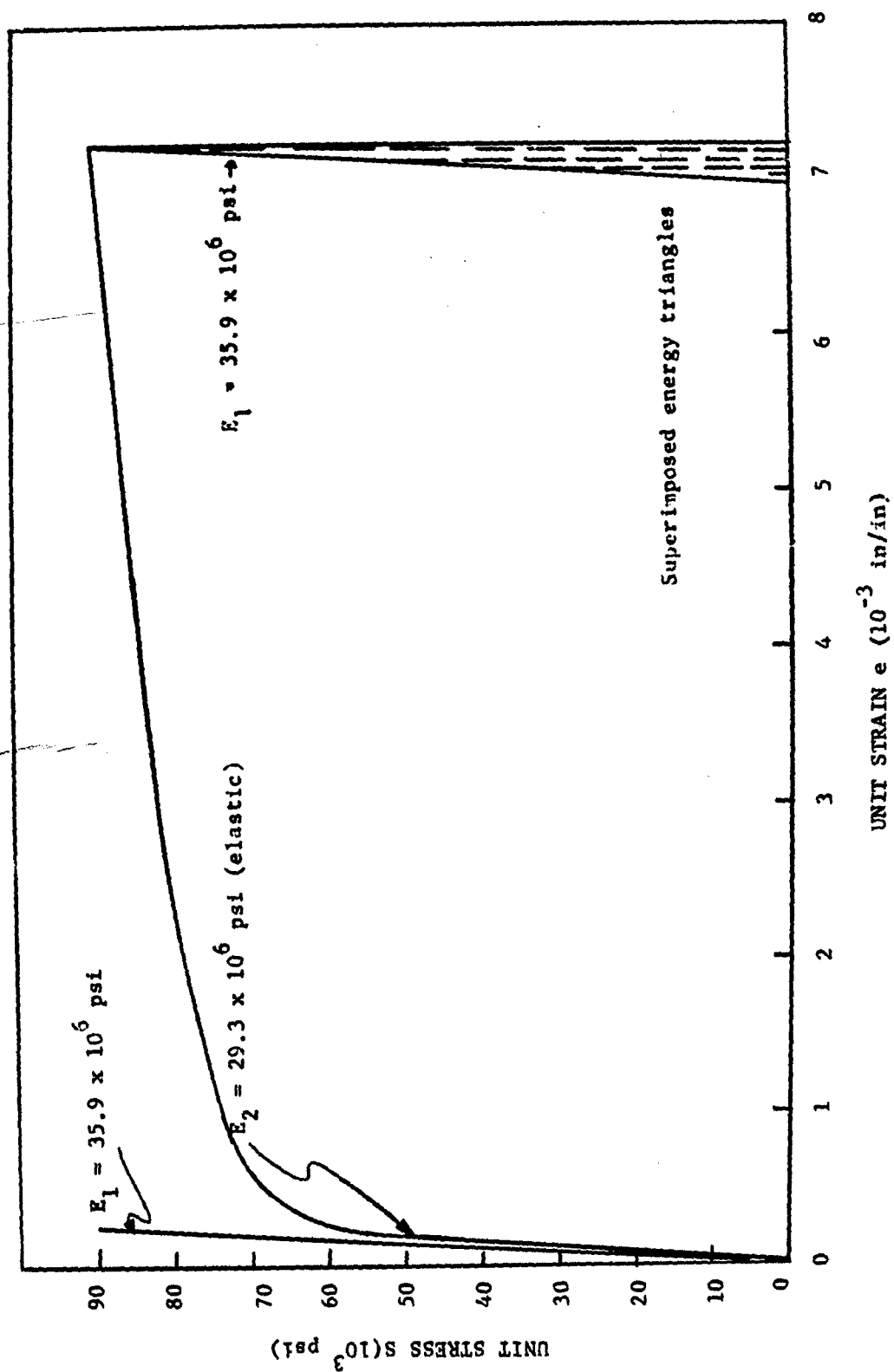Fig. 1.4. Unit stress plotted against unit strain for copper in compression. Specimens of 3/4" diameter and 2" long were used.
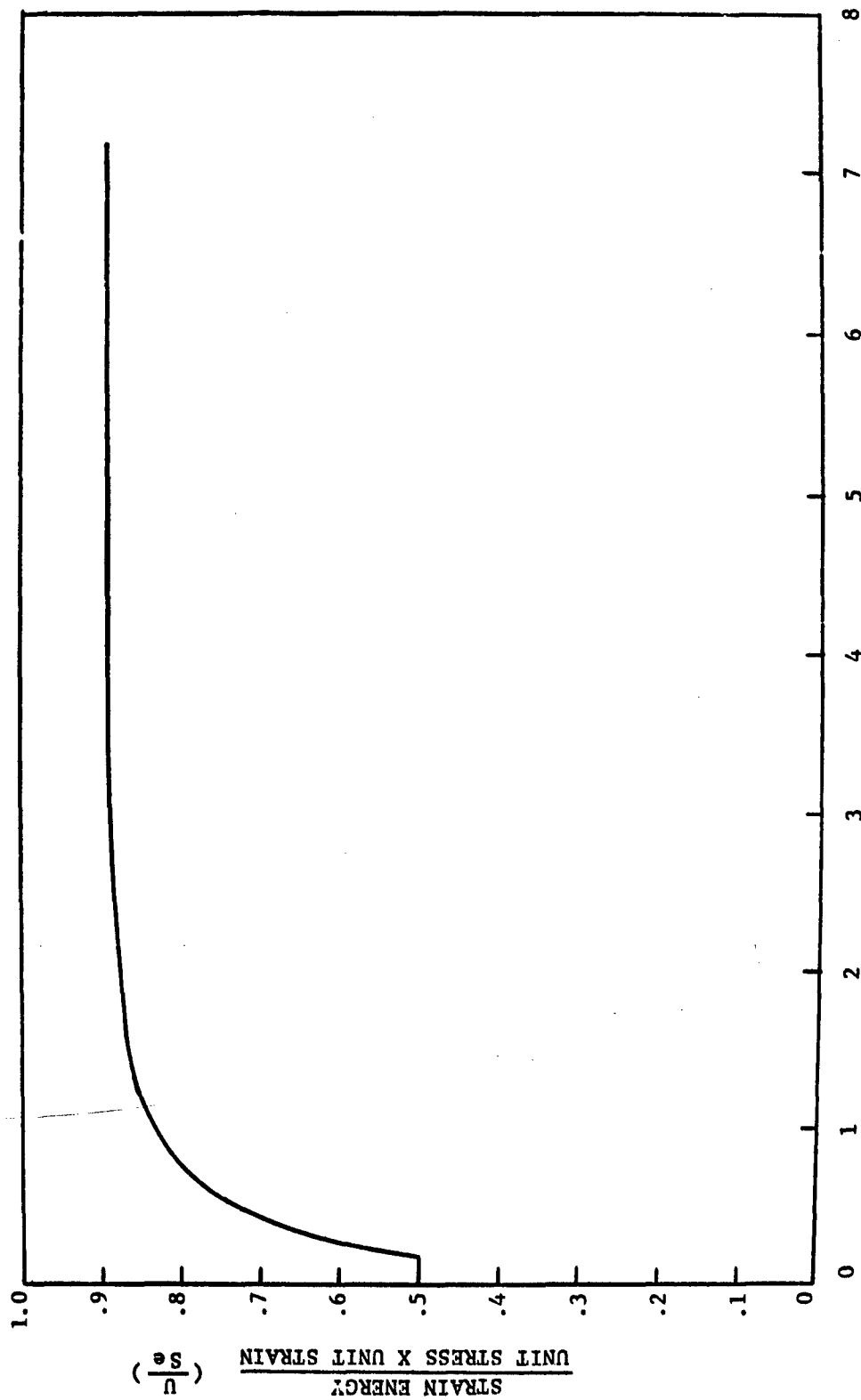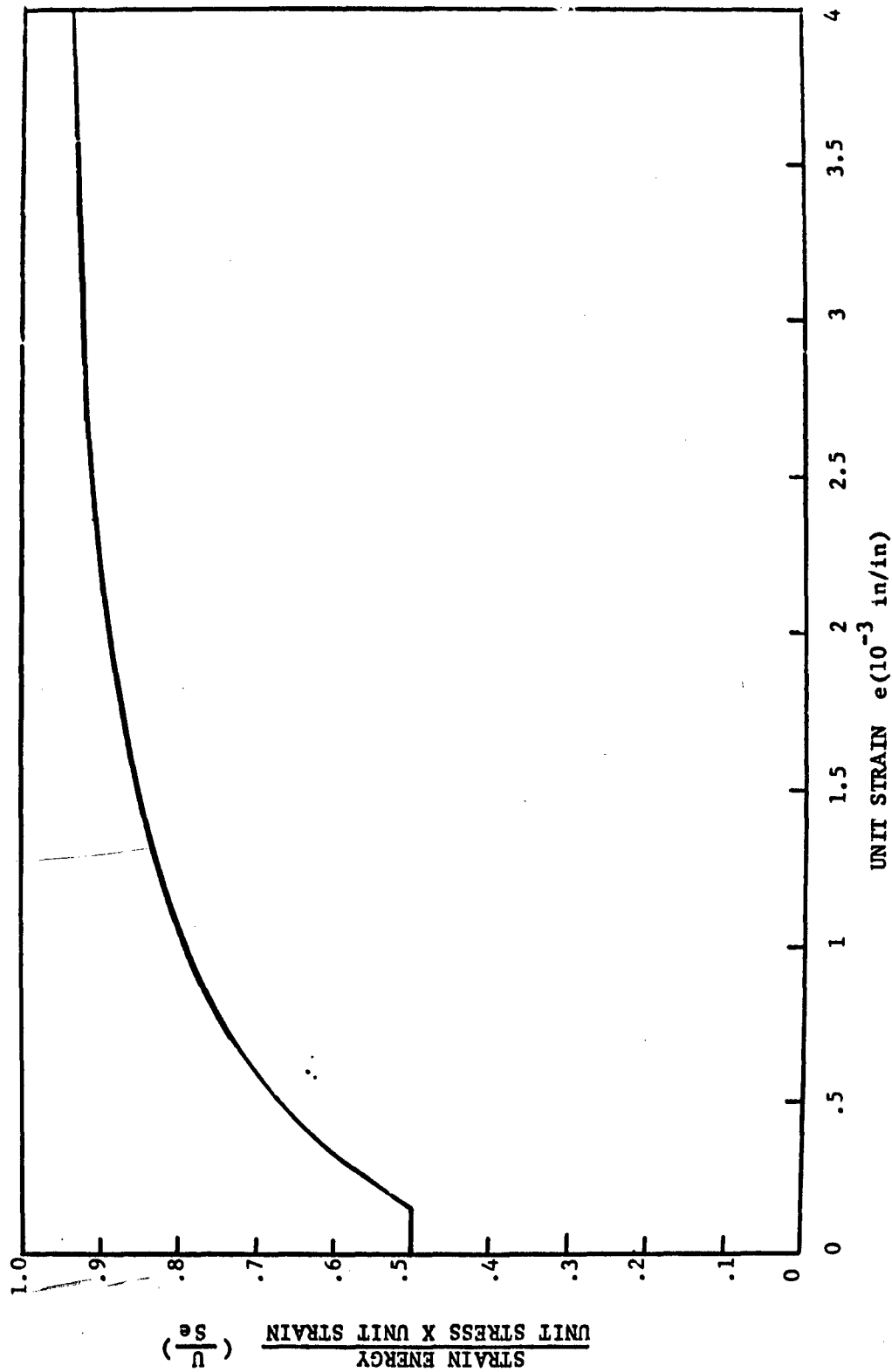
Fig. 1.4a. Strain energy divided by the unit stress times unit strain ($\frac{U}{Se}$) plotted against unit strain (e) for copper in compression. Specimens of 3/4" diameter and 2" long were used.
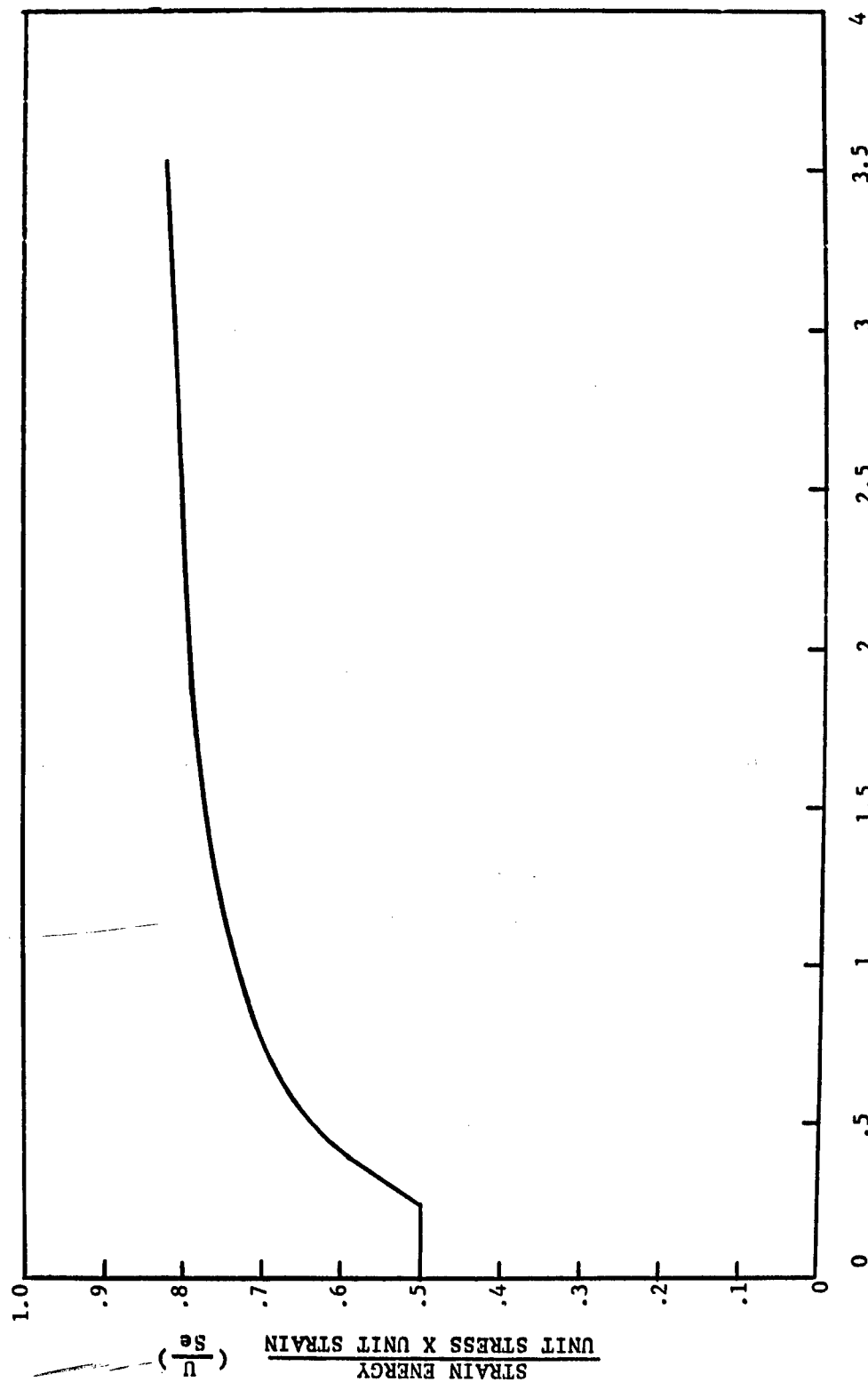
are the ultimate values. Such curves are illustrated by Fig. 1.5.
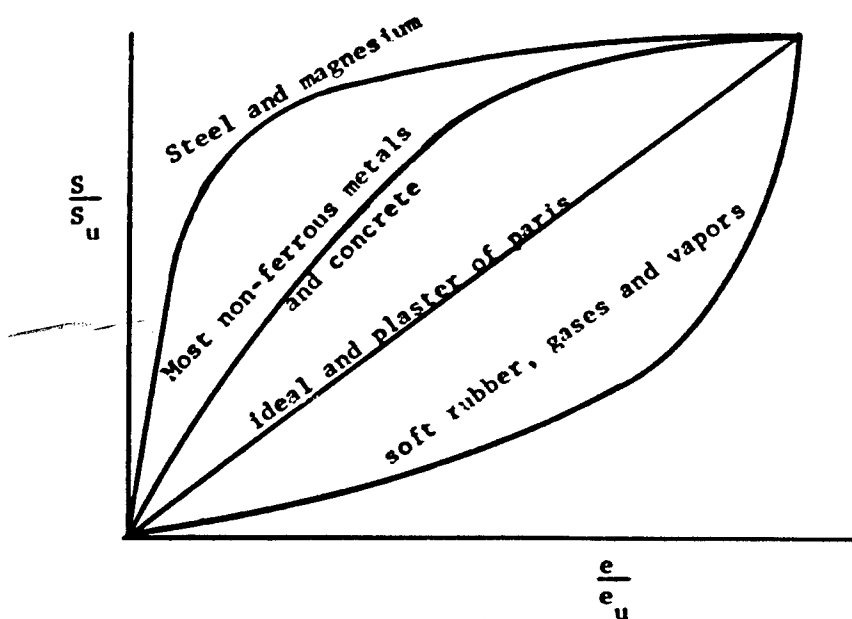
Fig. 1.5

For concrete, Talbot[1] had success with a parabolic equation between S/S_u and e/e_u but to cover all of the cases of Fig. 1.5, a more versatile equation is needed. The form of the curves of Fig. 1.5 suggests that they should be described in three variables. Actually, the stress S, the deformation e and the total stressing energy u per unit volume are all involved in wave action. These three variables can reasonably well be related by,

$$\frac{u}{Se} = c \tag{1.1}$$

where c is a characteristic constant for any family of materials. Since the internal energy is changed only by applied stress,

$$du = Sde \tag{1.2}$$

Equations 1 and 2 give

$$\int_{u_u}^{u} \frac{du}{u} = \frac{1}{c} \int_{e}^{e_u} \frac{de}{e} \tag{1.3}$$

$$\frac{u}{u_u} = \left(\frac{e}{e_u}\right)^{\frac{1}{c}} \tag{1.4}$$

$$\frac{S}{S_u} = \left(\frac{e}{e_u}\right)^{\frac{1-c}{c}} \tag{1.5}$$

$$\frac{u}{u_u} = \left(\frac{S}{S_u}\right)^{\frac{1}{1-c}} \tag{1.6}$$

As may be seen from Fig. 1.6, Eq. 1.5 does fit steel quite well in the hyper-elastic range. Actually, the degree to which Eq. 1.5 can be made to fit test stress-strain curves of metals is largely determined by the values of the ultimate stress S_u and ultimate deformation e_u that are used. As can be seen from Figs. 1.2, 1.3, and 1.4, the ultimate stress in compression is not clearly defined. However, such a formulation as that of Eq. 1.1 can be used to describe both linear and non-linear materials.

1.5 Waves in Linear Materials

Fig. 1.7

- 12 -
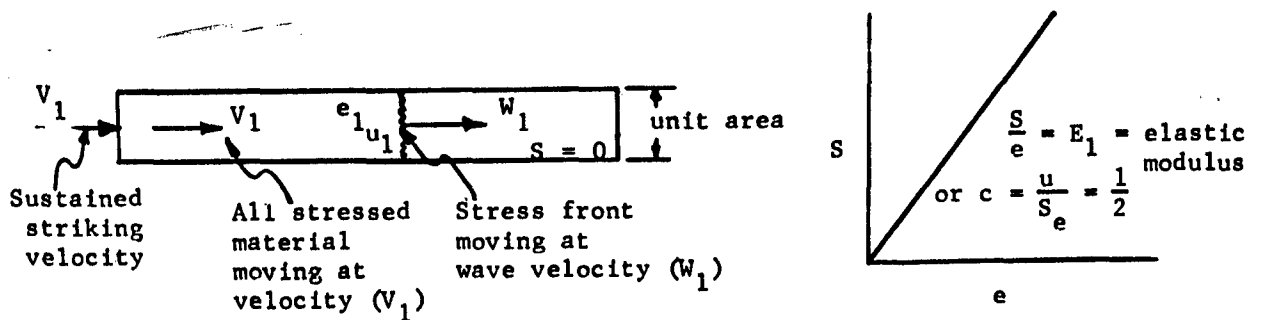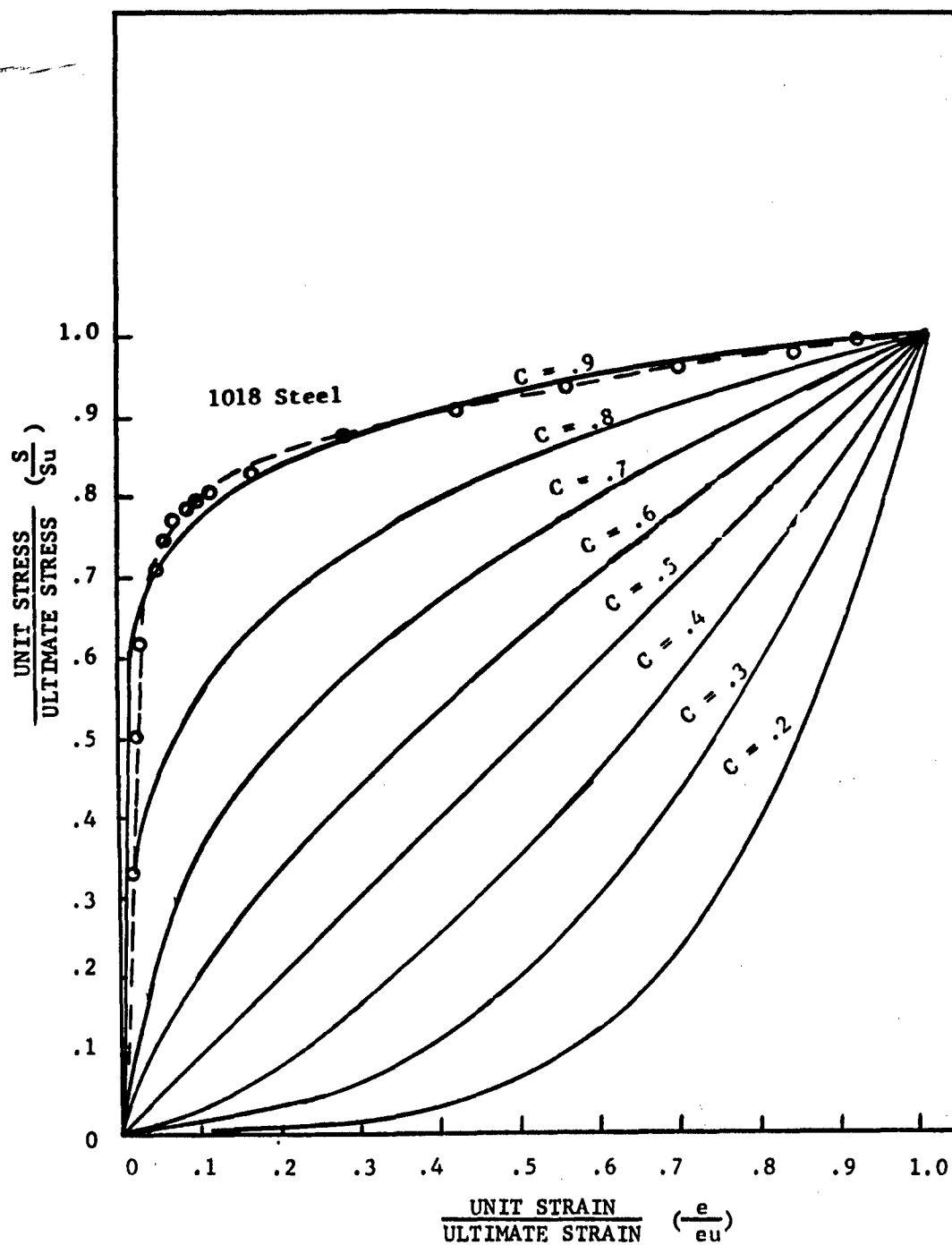
Fig. 1.6. Unit stress divided by ultimate stress plotted against unit strain divided by ultimate strain. Calculated from $\frac{U}{Se} = C$ and $dU = Sde$.

In the classical case of a stationary unstressed rod struck by a sustained impact velocity V_1, a stress wave moves through the material at a steady velocity W_1. Behind this front, the material is at a uniform stress S_1 with a unit deformation e_1 and moving at V_1. The wave processes W_1 cu.ft. per sec. of material and the transmitted power S_1V_1 reaching the front must give this material its internal energy u_1 and its kinetic energy per unit volume $\frac{\rho V_1^2}{2}$ so,

$$S_1V_1 = W_1 \left[u_1 + \frac{\rho V_1^2}{2} \right] \qquad (1.7)$$

The stress S_1 on the unit area must cause ρW_1 sluges per second to gain a velocity V_1 so

$$S_1 = \rho W_1 V_1 \qquad (1.8)$$

The velocity V_1 must be great enough to take up the slack resulting from the unit deformation e_1 or

$$V_1 = e_1 W_1 \qquad (1.9)$$

For a linear material with a modulus E_1

$$S_1 = E_1 e_1 \qquad (1.10)$$

and

$$u_1 = \frac{S_1^2}{2E_1} \qquad (1.11)$$

- 14 -

The result is the classical elastic wave equations,

$$W_1 = \sqrt{\frac{E_1}{\rho}} \tag{1.12}$$

and

$$S_1 = V_1 \sqrt{E_1 \rho} \tag{1.13}$$

1.6 Waves in Non-linear Materials

Since metals do have non-linear stress-strain curves in the hyper-elastic range, it becomes important to ask if single stress waves can be propagated through such materials. This can be investigated by replacing the linear Eqs. 1.10 and 1.11 by the non-linear Eq. 1.1. This can be done by using Eq. 1.1 in 1.7 to give

$$S_1 V_1 = W_1 (c S_1 e_1 + \frac{\rho V_1^2}{2}) \tag{1.14}$$

Using Eq. 1.8 to remove S_1

$$\rho W_1 V_1^2 = W_1 (c \rho W_1 V_1 e_1 + \frac{\rho V_1^2}{2}) \tag{1.15}$$

Further, using Eq. 1.9 to eliminate e_1 gives,

$$\rho W_1 V_1^2 = W_1 (\rho V_1^2 c + \frac{\rho V_1^2}{2}) \tag{1.16}$$

Equation 1.16 may be satisfied by $V_1 = 0$ or $W_1 = 0$ which, of course, is the condition for no wave. The only other solution is,

$$1 - c = \frac{1}{2} \quad \text{or} \quad c = \frac{1}{2} \tag{1.17}$$

- 15 -

From Fig. 1.6 this is the condition for a material with a linear stress-strain curve.

Before concluding that a single stress wave cannot propagate in a non-linear material, it should be recalled that in a gas with the non-linear curve of Fig. 1.5, shock waves are propagated. It is also known that the action in such shock fronts is highly turbulent. Turbulence in a solid material can be set up by arguing that the internal energy u of Eq. 1.1, Fig. 1.5, and Fig. 1.6 represents only the final energy mechanically stored. The amount of supplied energy to produce this would be greater than this fu_1 where f is a number greater than unity. This would mean that energy $\left[(1-f)u_1\right]$ would be lost as heat during the stressing process.

The space Eq. 1.9 would not be altered

$$V_1 = e_1 W_1 \tag{1.18}$$

However, the energy Eq. 1.7 would be

$$S_1 V_1 = W_1 \left[fu_1 + \frac{\rho V_1^2}{2} \right] \tag{1.19}$$

The force Eq. 1.8 would remain

$$S_1 = \rho W_1 V_1 \tag{1.20}$$

and the non-linear medium would be,

$$\frac{u_1}{S_1 e_1} = c \tag{1.21}$$

- 16 -

Combining these gives,

$$W_1 \rho V_1^2 = W_1 \rho V_1^2 \left[fe + \frac{1}{2} \right] \qquad (1.22)$$

Equation 1.22 can be satisfied for c greater than 1/2 only by a f less than unity and this cannot be. However, for c less than 1/2 (Fig. 1.6) there is a turbulence level depicted by f greater than unity for which a single wave front can propagate. Since for gases, c is less than 1/2 this bears our what is known about the high turbulence in gas shock waves.

All of this fits the following physical picture. For a linear material c = 1/2 the transmitted energy per sec. for a unit area $S_1 V_1$ which reaches the front is exactly the correct amount needed to supply the stress energy and the kinetic energy involved. Consequently, such a wave 's reversible and it can exist either as a compression wave or as a recovery or rarefaction wave. For a material, such as a gas, described by a c less than 1/2 the energy reaching the front $S_1 V_1$ is greater than that needed to supply the internal energy and the kinetic energy. Consequently, if there exists a mechanism for losing energy, (f greater than unity) a compression wave can occur, as it does in a gas. For a material such as the materials represented by c greater than 1/2, the amount of energy transmitted to the front is not enough to supply the required internal energy and kinetic energy, so such a wave cannot occur.

1.7 Hyper-Elastic Waves

For any analysis of hyper-elastic impact stresses to be valid, it must be capable of explaining certain physical observations.

a. When strain gage traces are determined near the impacted end of a bar A and at the center B, Fig. 1.8 illustrates typical results. When the impacting velocity V is near or below 30 ft. per sec., two things seem apparent on such films. The progress of the "toe" of the wave 1 is checked by the elastic velocity using the recovery modulus $\sqrt{\frac{E_1}{\rho}}$ of Table 1.1 and the full deformation point 2 is checked by the usual elastic modulus E_2 as $\sqrt{\frac{E_2}{\rho}}$. These two values of E are explained by Fig. 1.1. The rise time 1-2, corrected for strain gage length, becomes greater as the strain gage is moved down the bar. This suggests that such an elastic wave is, in reality, a zone and not a front.
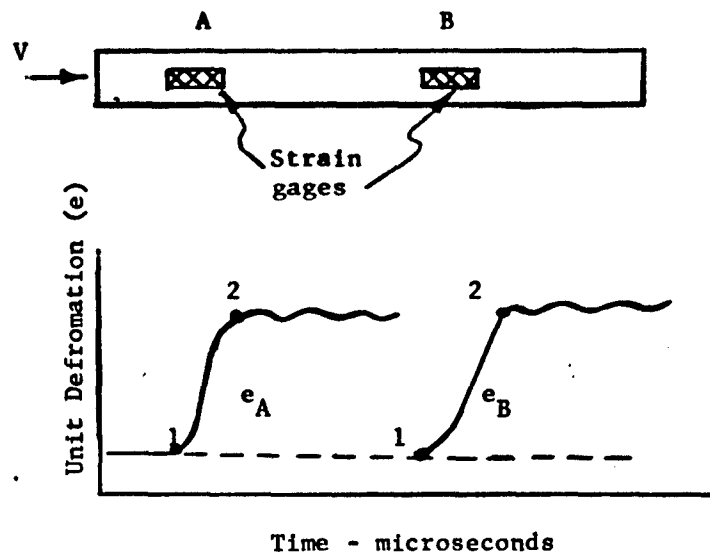

Fig. 1.8

- 18 -

b. When the impact velocity V is raised to 80 or 90 ft. per sec., the strain gage traces of Fig. 1.9 are typical. The first strain increase 1-2 remains essentially the same as in the low velocity case of Fig. 1.8. However, it is followed by a later very large strain which quickly goes off scale for gage A but rises more casually at position B. The deformation e_2 is consistently at or below the so-called elastic deformation of Figs. 1.2 to 1.4. The rate of rise of the following hyper-elastic deformation 2-3, Fig. 1.9, becomes progressively less along the bar.
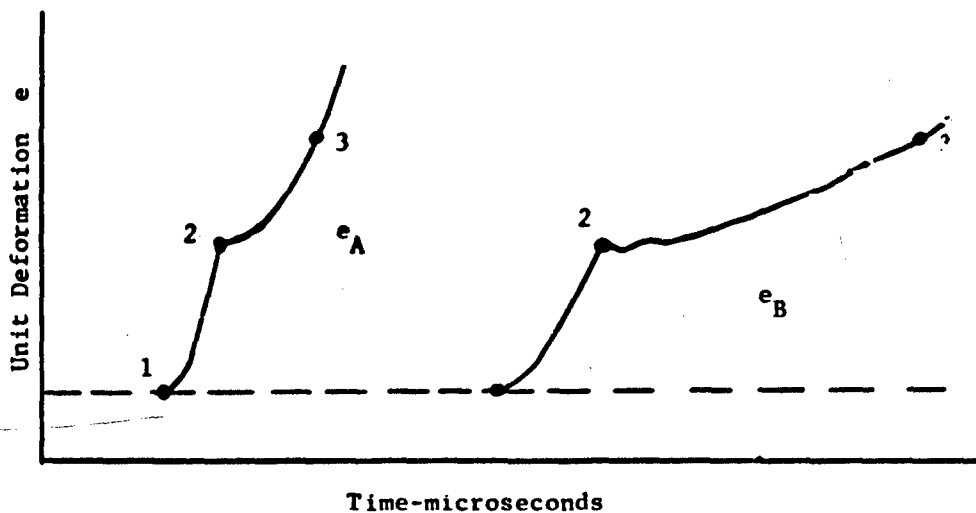
Fig. 1.9

The hyper-elastic wave hypothesis which appears to be consistent with all of these observations is illustrated by Figs. 1.10 and 1.11. When the bar of Fig. 1.11 is impacted, an elastic wave with a deformation e_1 travels along the bar. This is followed by a zone in which the elastic slip e_1 to e_2 occurs and the back of this zone moves down the bar at a

E$_2$ = elastic modulus

E$_1$ = recovery modulus

0 to 1 = elastic wave

1 to 2 = elastic slip

2 to 3 = hyper-elastic slip

Recovery energy

Fig. 1.10

W = Wave Velocity   V = Material Velocity

Fig. 1.11

velocity W_2. Finally this is followed by a hyper-elastic slip from e_2 to e_3, which brings the rod velocity up to the impact value V_3. At lower impact velocities, this last action can be absent.

- 20 -

1.8 Analysis of Hyper-Elastic Impacts

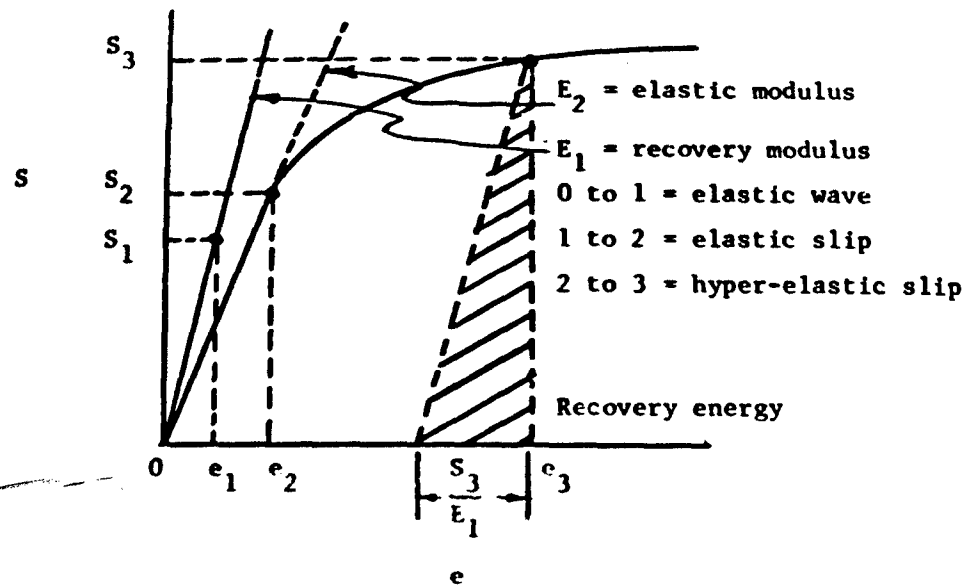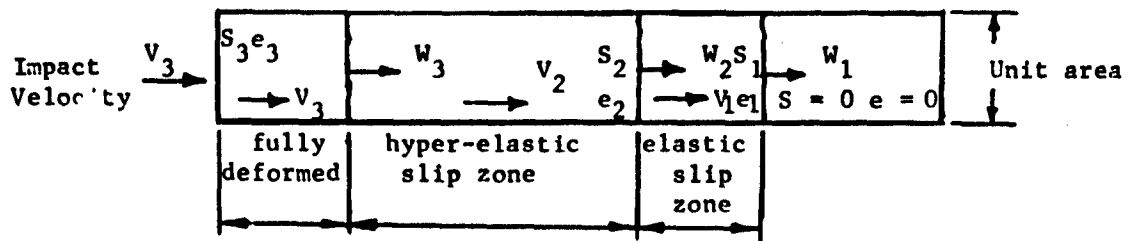For it to have engineering worth, the explanation of hyper-elastic impacts outlined in Article 1.7 must be expressed in numbers. Only then can it be verified and used.

a. **Elastic Wave 0-1.** Figures 1.10 and 1.11

From Eqs. 1.10, 1.12, and 1.13, article 1.5

$$S_1 = E_1 e_1 = V_1 \sqrt{E_1 \rho} \tag{1.23}$$

$$W_1 = \sqrt{\frac{E_1}{\rho}} \tag{1.24}$$

$$u_1 = \frac{S_1^2}{2E_1} = \frac{e_1 S_1}{2} \tag{1.25}$$

b. **Elastic Slip 1-2.** Figures 1.10 and 1.11

Test results illustrated by Figs. 1.8 and 1.9 suggest that the slip deformation 1-2 actually occurs in a zone at finite length. However, to keep mathematical complications from precluding a workable solution, the venerable "lump constant" method of reducing it to an equivalent discontinuity will be used.

This elastic slip wave moving at a velocity W_2 overtakes $(W_2 - V_1)$ cu. ft. per sec. of metal and increases its velocity from V_1 to V_2. A force balance gives,

$$\text{(Force)}, \quad S_2 - S_1 = \rho (W_2 - V_1)(V_2 - V_1) \tag{1.26}$$

- 21 -

The material $(W_2 - V_1)$ with a deformation e_1 must occupy space $(W_2 - V_2$ with a deformation e_2 or

$$\text{(Space)} \qquad (W_2 - V_1)(1 - e_2) = (W_2 - V_2)(1 - e_1) \qquad (1.27)$$

The transmitted energy per sec. S_2V_2 reaching the slip front must supply S_1V_1 transmitted to the elastic wave front and supply the internal energy and kinetic energy increase for $(W_2 - V_1)$ cu. ft. per sec. or

$$\text{(Energy)} \qquad S_2V_2 = S_1V_1 + (W_2 - V_1)\left[u_2 - u_1 + \frac{\rho v_2^2}{2} - \frac{\rho v_1^2}{2}\right] \qquad (1.28)$$

While the slip path 1-2 of Fig. 1.10 is not actually known, a reasonable approximation is

$$u_2 - u_1 = \frac{(S_1 + S_2)}{2}(e_2 - e_1) \qquad (1.29)$$

and, of course,

$$S_2 = E_2 e_2 \qquad (1.30)$$

Eliminating W_2 from Eqs. 1.26 and 1.27,

$$W_2 = V_1 + \frac{(S_2 - S_1)}{\rho(V_2 - V_1)} = \frac{V_2(1-e_1)-V_1(1-e_2)}{e_2 - e_1} \qquad (1.31)$$

Similarly, using Eq. 1.26 to eliminate $(W_2 - V_1)$ from Eq. 1.28,

$$S_2V_2 = S_1V_1 + \frac{(S_2 - S_1)}{\rho(V_2 - V_1)}\left[u_2 - u_1 + \frac{\rho v_2^2}{2} - \frac{\rho v_1^2}{2}\right] \qquad (1.32)$$

Using Eqs. 1.23 and 1.30 to eliminate S_1, V_1 and S_2 from Eq. 1.31,

$$W_2 = \sqrt{\frac{E_1}{\rho}}\, e_1 + \frac{(E_2 e_2 - E_1 e_1)}{\rho\left(V_2 - e_1\sqrt{\frac{E_1}{\rho}}\right)} = \frac{V_2(1 - e_1) - e_1\sqrt{\frac{E_1}{\rho}}\,(1 - e_2)}{(e_2 - e_1)} \quad (1.33)$$

Using Eqs. 1.23, 1.29, and 1.30 to eliminate S_1, V_1, u_2 and S_2 from Eq. 1.32,

$$E_2 e_2 V_2 = E_1 e_1^2\sqrt{\frac{E_1}{\rho}} + \frac{(E_2 e_2 - E_1 e_1)}{\rho\left(V_2 - e_1\sqrt{\frac{E_1}{\rho}}\right)}\left[\frac{(E_1 e_1 + E_2 e_2)}{2}(e_2 - e_1)\right.$$

$$\left. + \frac{\rho V_2^2}{2} - \frac{E_1 e_1^2}{2}\right] \quad (1.34)$$

Clearing Eq. 1.33

$$e_1\sqrt{E_1\rho}\,(e_2 - e_1)\left(V_2 - e_1\sqrt{\frac{E_1}{\rho}}\right) + (E_2 e_2 - E_1 e_1)(e_2 - e_1) =$$

$$\rho V_2(1 - e_1)\left(V_2 - e_1\sqrt{\frac{E_1}{\rho}}\right) - e_1\sqrt{E_1\rho}\,(1 - e_2)\left(V_2 - e_1\sqrt{\frac{E_1}{\rho}}\right) \quad (1.35)$$

Collecting terms in Eq. 1.35,

$$\rho(1 - e_1)V_2^2 - V_2\left[e_1\sqrt{E_1\rho}\,(1 - e_2) + \rho(1 - e_1)e_1\sqrt{\frac{E_1}{\rho}} + e_1\sqrt{E_1\rho}\,(e_2 - e_1)\right.$$

$$+ e_1^2 E_1(1 - e_2) - (E_2 e_2 - E_1 e_1)(e_2 - e_1) + E_1 e_1^2(e_2 - e_1) = 0 \quad (1.36)$$

or

$$V_2^2 - 2\sqrt{\frac{E_1}{\rho}}\, e_1 V_2 + \frac{E_1 e_1^2(1 - e_1) - (E_2 e_2 - E_1 e_1)(e_2 - e_1)}{\rho(1 - e_1)} = 0 \quad (1.37)$$

- 23 -

Clearing Eq. 1.34

$$2\rho(V_2 - e_1\sqrt{\frac{E_1}{\rho}})E_2 e_2 V_2 = 2E_1 e_1^2 \rho\sqrt{\frac{E_1}{\rho}}(V_2 - e_1\sqrt{\frac{E_1}{\rho}})$$

$$+ (E_2 e_2 - E_1 e_1)\left[(E_1 e_1 + E_2 e_2)(e_2 - e_1) + \rho V_2^2 - E_1 e_1^2\right] \qquad (1.38)$$

Collecting terms in Eq. 1.38,

$$\rho V_2^2\left[2E_2 e_2 - E_2 e_2 - E_1 e_1\right] - \rho V_2\left[2e_1 e_2 E_2\sqrt{\frac{E_1}{\rho}} + 2E_1 e_1^2\sqrt{\frac{E_1}{\rho}}\right]$$

$$+ 2E_1^2 e_1^3 - (E_2 e_2 - E_1 e_1)\left[(E_1 e_1 + E_2 e_2)(e_2 - e_1) - E_1 e_1^2\right] = 0 \qquad (1.39)$$

or

$$V_2^2 - 2\sqrt{\frac{E_1}{\rho}}e_1 V_2 + \frac{2E_1^2 e_1^3 - \left[E_2 e_2 - E_1 e_1\right]\left[(E_2 e_2 + E_1 e_1)(e_2 - e_1) - E_1 e_1^2\right]}{\rho\left[E_2 e_2 + E_1 e_1\right]} = 0$$

$$(1.40)$$

Since Eq. 1.37 combines the force and space equations and Eq. 1.40 combines the force and energy equations, their simultaneous solution describes the conditions that must be met by the elastic slip front, 1-2 Fig. 1.11, to enable it to drive the elastic wave 1 ahead of it.

Eliminating V_2 from Eqs. 1.37 and 1.40,

$$\frac{E_1 e_1^2(1 - e_1) - (E_2 e_2 - E_1 e_1)(e_2 - e_1)}{\rho(1 - e_1)} =$$

$$\frac{2E_1^2 e_1^3 - \left[E_2 e_2 - E_1 e_1\right]\left[(E_2 e_2 + E_1 e_1)(e_2 - e_1) - E_1 e_1^2\right]}{\rho\left[E_2 e_2 + E_1 e_1\right]} \qquad (1.41)$$

- 24 -

Clearing Eq. 1.41

$$E_1 e_1^2 (1-e_1) \left[E_2 e_2 + E_1 e_1 \right] - (E_2 e_2 - E_1 e_1)(E_2 e_2 + E_1 e_1)(e_2 - e_1) =$$

(1.42)

$$2E_1^2 e_1^3 (1-e_1) - (E_2 e_2 - E_1 e_1)(E_2 e_2 + E_1 e_1)(e_2 - e_1)(1-e_1) + (E_2 e_2 - E_1 e_1)E_1 e_1^2 (1-e_1)$$

Simplifying Eq. 1.42 gives

$$(E_2 e_2 + E_1 e_1)(E_2 e_2 - E_1 e_1)(e_2 - e_1) =$$

$$(E_2 e_2 + E_1 e_1)(E_2 e_2 - E_1 e_1)(e_2 - e_1)(1-e_1) \qquad (1.43)$$

Equation 1.43 has three possible solutions,

a. $(1 - e_1) = 1$ or $e_1 = 0$

b. $(e_2 - e_1) = 0$ or $e_2 = e_1$ (1.45)

c. $E_2 e_2 - E_1 e_1 = 0$ or $S_2 = S_1$ (1.46)

Of the three, $e_1 = 0$ seems to fit all observed conditions. When $e_1 = 0$ is used in Eq. 1.37, the result is

$$V_2 = e_2 \sqrt{\frac{E_2}{\rho}} \qquad (1.47)$$

Using this value of V_2 and $e_1 = 0$ in Eq. 1.31 gives,

$$W_2 = \frac{V_2}{e_2} = \sqrt{\frac{E_2}{\rho}} \qquad (1.48)$$

This value of W_2 in conjunction with $W_1 = \sqrt{\frac{E_1}{\rho}}$ from Eq. 1.24 goes

- 25 -

a long way toward explaining the fact illustrated in Figs. 1.8 and 1.9 that measured deformations bear little resemblance to classical square wave fronts.

Remembering that the "lump constant" method here used is really attempting to describe what is probably a deformation zone, the following picture begins to make sense. If the front of this zone travels at $W_1 = \sqrt{E_1/\rho}$ and the rear of it at $W_2 = \sqrt{E_2/\rho}$, the zone will get progressively longer as it travels along the bar because W_1 is greater than W_2. As illustrated by Figs. 1.8 and 1.9, this explains why the deformation front becomes longer and flatter as the disturbance travels along the bar.

c. **Hyper-Elastic Slip 2-3**

The hyper-elastic slip 2-3 of Fig. 1.10 occurs progressively over a varying length so its reduction to a single "lump constant" effect will have to be based on average conditions. The average deformation in the slip zone may be taken as $\dfrac{e_2 + e_3}{2}$ and the average material velocity in the zone is $\dfrac{V_2 + V_3}{2}$. The average energy increase would be taken as half of the maximum value. On this basis the force, space, and energy equations corresponding to Eqs. 1.26, 1.27, and 1.28 become

Force
$$S_3 = S_2 = \rho(W_3 - V_2)\left(\frac{V_3 - V_2}{2}\right) \tag{1.49}$$

Space
$$(W_3 - V_2)\left[1 - \frac{(e_3 + e_2)}{2}\right] = (W_3 - V_3)(1 - e_2) \tag{1.50}$$

Energy
$$S_3 V_3 = S_2 V_2 + (W_3 - V_2)\frac{1}{2}\left[u_3 - u_2 + \frac{\rho V_3^2}{2} - \frac{\rho V_2^2}{2}\right] \tag{1.51}$$

While the relationship between V_2 and e_2 is determined by Eqs. 1.40 and the choice of one of Eqs. 1.44, 1.45, or 1.46, it is known that,

$$S_2 = E_2 e_2 \quad \text{and} \quad u_2 = \frac{S_2^2}{2E_2^2} = \frac{E_2 e_2^2}{2} \quad (1.52)$$

so

Force
$$S_3 - E_2 e_2 = \rho(W_3 - V_2)\left(\frac{V_3 - V_2}{2}\right) \quad (1.53)$$

Space
$$(W_3 - V_2)(1 - e_{3/2} - e_{2/2}) = (W_3 - V_3)(1 - e_2) \quad (1.54)$$

Energy
$$S_3 V_3 = E_2 e_2 V_2 + (W_3 - V_2)\frac{1}{2}\left[u_3 - \frac{E_2 e_2^2}{2} + \frac{\rho V_3^2}{2} - \frac{\rho V_2^2}{2}\right] \quad (1.55)$$

Eliminating W_3 from Eqs. 1.53 and 1.54

$$W_3 = V_2 + \frac{2(S_3 - E_2 e_2)}{\rho(V_3 - V_2)} = \frac{V_3(1 - e_2) - V_2(1 - e_{2/2} - e_{3/2})}{(e_{3/2} - e_{2/2})} \quad (1.56)$$

Using Eq. 1.53 to eliminate $(W_3 - V_2)$ from Eq. 1.55,

$$S_3 V_3 = E_2 e_2 V_2 + \frac{(S_3 - E_2 e_2)}{\rho(V_3 - V_2)}\left[u_3 - \frac{E_2 e_2^2}{2} + \frac{\rho V_3^2}{2} - \frac{\rho V_2^2}{2}\right] \quad (1.57)$$

Clearing Eq. 1.56

$$\rho V_2(V_3 - V_2)(e_{3/2} - e_{2/2}) + 2(S_3 - E_2 e_2)(e_{3/2} - e_{2/2}) =$$

$$\rho V_3(1 - e_2)(V_3 - V_2) - \rho V_2(V_3 - V_2)(1 - e_{2/2} - e_{3/2}) \quad (1.58)$$

- 27 -

Collecting terms in Eq. 1.58

$$(1-e_2)\rho V_3^2 - (1-e_2)2\rho V_2 V_3 + \rho V_2^2(1-e_2) - (S_3-E_2 e_2)(e_3-e_2) = 0 \qquad (1.59)$$

or

$$V_3^2 - 2V_2 V_3 + \frac{\rho V_2^2(1-e_2)-(S_3-E_2 e_2)(e_3 - e_2)}{\rho(1 - e_2)} = 0 \qquad (1.60)$$

Clearing Eq. 1.57

$$\rho V_3(V_3-V_2)S_3 = \rho V_2(V_3-V_2)E_2 e_2 + (S_3-E_2 e_2)\left[u_3 - \frac{E_2 e_2^2}{2} + \frac{\rho V_3^2}{2} - \frac{\rho V_2^2}{2}\right]$$

$$(1.61)$$

Collecting terms in Eq. 1.61

$$\rho V_3^2 \frac{(S_3 + E_2 e_2)}{2} - \rho V_2(S_3+E_2 e_2)V_3 + \rho V_2^2 E_2 e_2 - (S_3-E_2 e_2)(u_3 - \frac{E_2 e_2^2}{2} - \frac{\rho V_2^2}{2}) = 0$$

or $$(1.62)$$

$$V_3^2 - 2V_2 V_3 + \frac{2\rho V_2^2 E_2 e_2 - 2(S_3 - E_2 e_2)(u_3 - \frac{E_2 e_2^2}{2} - \frac{\rho V_2^2}{2})}{\rho(S_3 + E_2 e_2)} = 0 \qquad (1.63)$$

Eliminating V_3 between Eqs. 1.60 and 1.63

$$\frac{\rho V_2^2(1-e) - (S_3-E_2 e_2)(e_3-e_2)}{\rho(1-e_2)} = \frac{2\rho V_2^2 E_2 e_2 - 2(S_3-E_2 e_2)(u_3 - \frac{E_2 e_2^2}{2} - \frac{\rho V_2^2}{2})}{\rho(S_3 + E_2 e_2)} \qquad (1.64)$$

Clearing Eq. 1.64

$$\rho V_2^2(1-e_2)(S_3-E_2 e_2) - (S_3-E_2 e_2)(e_3-e_2)(S_3 + E_2 e_2) =$$

$$-(1-e_2)(S_3-E_2 e_2)(2u_3-E_2 e_2^2 - \rho V_2^2) \qquad (1.65)$$

or

$$(S_3 - E_2 e_2)(e_3 - e_2)(S_3 + E_2 e_2) = (1 - e_2)(S_3 - E_2 e_2)(2u_3 - E_2 e_2^2) \qquad (1.66)$$

One solution is

$$S_3 - E_2 e_2 = 0 \qquad \text{or} \qquad S_3 = E_2 e_2 \qquad (1.67)$$

Which is the case of no hyper-elastic slip. This leaves,

$$(e_3 - e_2)(S_3 + E_2 e_2) = (1 - e_2)(2u_3 - E_2 e_2^2) \qquad (1.68)$$

Since e_2 will not exceed .003, the $(1 - e_2)$ multiplying factor may safely be used as 1.00 and a cubic equation avoided. In that way,

$$e_2 = \frac{e_3 \left[\dfrac{2u_3}{S_3 e_3} - 1 \right]}{\dfrac{E_2 e_3}{S_3} - 1} \qquad (1.69)$$

Using $V_2 = e_2 \sqrt{\dfrac{E_2}{\rho}}$ from Eq. 1.47 in Eq. 1.60 and again letting the multiplying factor $(1 - e_2)$ be replaced by 1.00 gives,

$$\frac{V_3}{\sqrt{\dfrac{E_2}{\rho}}} = e_2 \pm \sqrt{(e_3 - e_2)(\frac{S_3}{E_2} - e_2)} \qquad (1.70)$$

- 29 -

Similarly, from Eq. 1.56

$$\frac{W_3}{\sqrt{\frac{E_2}{\rho}}} = \frac{2\left(\sqrt{\frac{V_3}{E_2/\rho}} - e_2\right)}{(e_3 - e_2)} = \frac{2\sqrt{(e_3 - e_2)\left(\frac{S_3}{E_2} - e_2\right)}}{(e_3 - e_2)} \qquad (1.71)$$

or

$$\frac{W_3}{\sqrt{\frac{E_3}{\rho}}} = 2\sqrt{\frac{(S_3/E_2 - e_2)}{(e_3 - e_2)}} \qquad (1.72)$$

Hyper-elastic waves can be summarized by

$$\frac{V_2}{\sqrt{E_2/\rho}} = e_2 \qquad (1.73)$$

$$\frac{V_3}{\sqrt{E_2/\rho}} = e_2 \pm \sqrt{(e_3 - e_2)\left(\frac{S_3}{E_2} - e_2\right)} \qquad (1.74)$$

$$e_2 = \frac{e_3\left[2\,\frac{u_3}{S_3 e_3} - 1\right]}{\left(\frac{E_2 e_3}{S_3} - 1\right)} \qquad (1.75)$$

$$\frac{W_3}{\sqrt{E_2/\rho}} = 2\sqrt{\frac{S_3/E_2 - e_2}{e_3 - e_2}} \qquad (1.76)$$

$$W_2 = \sqrt{E_2/\rho} \qquad (1.77)$$

$$W_1 = \sqrt{E_1/\rho} \qquad (1.78)$$

1.9 Proof of Proposed Test Method

The analysis of Article 1.8 was concerned with an investigation of the elastic and slip waves in a bar struck by a sustained velocity V_3 at one end. The classical simulation of this in the elastic range is to have a bar moving at a velocity V_3 strike an imagined stationary and rigid surface. However, since a moving bar shot from a gun cannot be instrumented with strain gages, another approach is needed.

The method used was to strike a stationary instrumented bar squarely with an exact image bar moving at a velocity of $2V_3$. Before this approach can be accepted, it must be demonstrated to be valid for the case of the elastic and slip waves of Article 1.8.
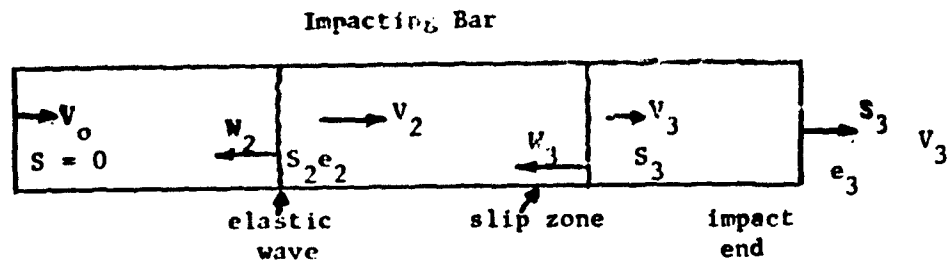
Impacting Bar

Fig. 1.12

This will be proven if the impacting bar of Fig. 1.12 moving at V_o has the same stress waves as those of Article 1.8 when the velocity of the impacting end is suddenly reduced to $V_3 = V_o/2$ by impact with the identical instrumented bar.

For the elastic wave:

Force: $$S_2 = (W_2 + V_o)\rho(V_o - V_2) \tag{1.79}$$

Space: $$(W_2 + V_o)(1 - e_2) = (W_2 + V_2) \tag{1.80}$$

Energy:
$$(W_2 + V_o)\left[\frac{\rho V_o^2}{2} - \frac{\rho V_2^2}{2} - u_2 = S_2 V_2\right] \tag{1.81}$$

Material:
$$S_2 = e_2 E_2 \text{ and } u_2 = \frac{S_2 e_2}{2} = \frac{E_2 e_2^2}{2} \tag{1.82}$$

Using Eq. 1.82 to eliminate S_2 and u_2 from Eqs. 1.79, 1.80, and 1.81,

Force:
$$E_2 e_2 = (W_2 + V_o)\rho(V_o - V_2) \tag{1.83}$$

Space:
$$(W_2 + V_o)(1-e_2) = (W_2 + V_2) \tag{1.84}$$

Energy:
$$(W_2 + V_o)\left[\frac{\rho V_o^2}{2} - \frac{\rho V_2^2}{2} - \frac{E_2 e_2^2}{2}\right] = E_2 e_2 V_2 \tag{1.85}$$

Eliminating W_2 from Eqs. 1.83 and 1.84

$$W_2 = \frac{E_2 e_2}{\rho(V_o - V_2)} - V_o = \frac{V_o(1-e_2) - V_2}{e_2} \tag{1.86}$$

Similarly, from Eqs. 1.83 and 1.84

$$\frac{E_2 e_2}{\rho(V_o - V_2)}\left[\frac{\rho V_o^2}{2} - \frac{\rho V_2^2}{2} - \frac{E_2 e_2^2}{2}\right] = E_2 e_2 V_2 \tag{1.87}$$

From Eq. 1.86

$$E_2 e_2^2 = \rho(V_o^2 - 2V_o V_2 + V_2^2) = \rho(V_o - V_2)^2 \tag{1.88}$$

or

$$e_2\sqrt{\frac{E_2}{\rho}} = (V_o - V_2) \tag{1.89}$$

- 32 -

Simplifying Eq. 1.87 also gives

$$e_2 \sqrt{\frac{E_2}{\rho}} = (V_o - V_2) \tag{1.90}$$

So

$$S_2 = E_2 e_2 = (V_o - V_2)\sqrt{E_2 \rho} \tag{1.91}$$

Now, for the average conditions in the slip zone of Fig. 1.12, the front moves at a velocity W_2 and the back of it at W_3. The average increase in velocity is $\frac{(V_2 - V_3)}{2}$ and the average unit deformation is $\frac{(e_3 + e_2)}{2}$.

Force: $\quad (S_3 - S_2) = \rho(W_3 + V_2)\dfrac{(V_2 - V_3)}{2} \tag{1.92}$

Space: $\quad (W_3 + V_2)\left[1 - \dfrac{(e_3 + e_2)}{2}\right] = (W_3 + V_3)(1 - e_3) \tag{1.93}$

Energy: $\quad S_2 V_2 - S_3 V_3 = (W_3 + V_2)\dfrac{1}{2}\left[u_3 - u_2 + \dfrac{\rho V_3^2}{2} - \dfrac{\rho V_2^2}{2}\right] \tag{1.94}$

Using

$$S_2 = E_2 e_2; \qquad u_2 = \frac{S_2 e_2}{2} = \frac{E_2 e_2^2}{2} \tag{1.95}$$

and from Eq. 1.90,

$$V_2 = V_o - e_2 \sqrt{\frac{E_2}{\rho}} \tag{1.96}$$

in Eqs. 1.92, 1.93, and 1.94.

Force: $\quad S_3 - E_2 e_2 = \rho\left[W_3 + V_o - e_2\sqrt{\frac{E_2}{\rho}}\right]\left[\dfrac{V_o - e_2\sqrt{\frac{E_2}{\rho}} - V_3}{2}\right] \tag{1.97}$

- 33 -

<u>Space:</u> $\left[W_3 + V_o - e_2\sqrt{\dfrac{E_2}{\rho}}\right]\left[1 - \dfrac{(e_3+e_2)}{2}\right] = (W_3 + V_3)(1-e_3)$ (1.98)

<u>Energy:</u> $E_2 e_2\left(V_o - e_2\sqrt{\dfrac{E_2}{\rho}}\right) - S_3 V_3 = \dfrac{1}{2}\left[W_3 + V_o - e_2\sqrt{\dfrac{E_2}{\rho}}\right]\left[u_3 - \dfrac{E_2 e_2^2}{2}\right.$

$$\left. + \dfrac{\rho V_3^2}{2} - \rho\left(V_o - e_2\sqrt{\dfrac{E_2}{\rho}}\right)^2\right] \qquad (1.99)$$

Eliminating W_3 from Eqs. 1.97 and 1.98

$$W_3 = \dfrac{2(S_3 - E_2 e_2)}{\rho\left[V_o - e_2\sqrt{\dfrac{E_2}{\rho}} - V_3\right]} - V_o + e_2\sqrt{\dfrac{E_2}{\rho}} = \dfrac{\left(V_o - e_2\sqrt{\dfrac{E_2}{\rho}}\right)\left[1 - \dfrac{(e_3+e_2)}{2}\right] - V_3(1-e_2)}{\dfrac{1}{2}(e_3 - e_2)} \qquad (1.100)$$

Using the value of $\dfrac{1}{2}\left(W_3 + V_o - e_2\sqrt{\dfrac{E_2}{\rho}}\right)$ from Eq. 1.97 in Eq. 1.99 gives,

$$E_2 e_2\left(V_o - e_2\sqrt{\dfrac{E_2}{\rho}}\right) - S_3 V_3 = \dfrac{(S_3 - E_2 e_2)\left[u_3 - \dfrac{E_2 e_2^2}{2} + \dfrac{\rho V_3^2}{2} - \rho\left(V_o - e_2\sqrt{\dfrac{E_2}{\rho}}\right)^2\right]}{\rho\left[V_o - e_2\sqrt{\dfrac{E_2}{\rho}} - V_3\right]} \qquad (1.101)$$

The desired proof can be established by solving for $\left[V_o - e_2\sqrt{\dfrac{E_2}{\rho}} - V_3\right]^2$ from Eqs. 1.100 and 1.101.

Doing this for Eq. 1.100 gives,

$$\left[V_o - e_2\sqrt{\dfrac{E_2}{\rho}} - V_3\right]^2 = \dfrac{(e_3 - e_2)(S_3 - E_2 e_2)}{\rho(1-e_2)} \qquad (1.102)$$

Similarly from Eq. 1.101,

$$\left[V_o - e_2\sqrt{\dfrac{E_2}{\rho}} - V_3\right]^2 = \dfrac{(S_3 - E_2 e_2)(2u_3 - E_2 e_2^2)}{\rho(S_3 + E_2 e_2)} \qquad (1.103)$$

- 34 -

Equating Eqs. 1.102 and 1.103 gives

$$\frac{(e_3-e_2)(S_3-E_2e_2)}{\rho(1-e_2)} = \frac{(S_3-E_2e_2)(2u_3-E_2e_2^2)}{\rho(S_3 + E_2e_2)} \qquad (1.104)$$

Conceling the root $S_3 = E_2e_2$ which is that of a wave in the elastic range and not of present concern, gives

$$\frac{2u_3 - E_2e_2^2}{S_3 + E_2e_2} = \frac{(e_3 - e_2)}{(1 - e_2)} \qquad (1.105)$$

Since this is exactly the conclusion reached in Eq. 1.68 of the original slip wave analysis, the value of $\dfrac{(S_3-E_2e_2)(e_3 - e_2)}{\rho(1-e_2)}$ from Eq. 1.60 may be used in Eq. 1.102 to give

$$V_3^2 - 2V_2V_3 + V_2^2 = \left[V_o - e_2\sqrt{\frac{E_2}{\rho}} - V_3\right]^2 \qquad (1.106)$$

But, from Eq. 1.47

$$e_2\sqrt{\frac{E_2}{\rho}} = V_2 \qquad (1.107)$$

So

$$V_3 - e_2\sqrt{\frac{E_2}{\rho}} = V_o - e_2\sqrt{\frac{E_2}{\rho}} - V_3 \qquad (1.108)$$

or

$$V_3 = \frac{V_o}{2} \qquad (1.109)$$

which is the necessary condition for the validity of the impacting bar scheme of Fig. 1.12.

- 35 -

1.10 Interpretation of Analytical Conclusions

The picture that has been contrived is that of the front of an inelastic slip zone traveling as an elastic wave at velocity $W_2 = \sqrt{E_2/\rho}$ and with deformation e_2. The imagined rear of this slip zone where the material has reached the full impacting velocity V_3 is moving at a velocity W_3, which, from Eq. 1.76, is usually much less than W_2. This slip zone of varying length has unit deformation e_2 at the front, e_3 at the back and was calculated by assuming a linear average of the kinetic energy and internal energy of the material in the slip zone.

As was described by Eq. 1.44 and illustrated by Fig. 1.10, this front traveling elastic wave has a slightly varying thickness as it travels along a rod. The front of it is traveling at $W_1 = \sqrt{E_1/\rho}$ and the rear at $W_2 = \sqrt{E_2/\rho}$, where E_1 is the truly elastic or recovery modulus of the material and E_2 is the commonly used elastic modulus of the material.
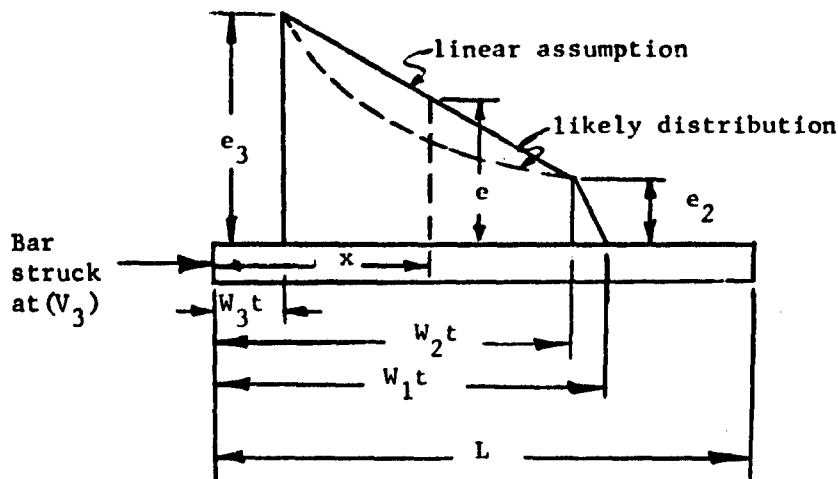

Fig. 1.13

- 36 -

The space distribution of unit deformation along a struck rod is illustrated by Fig. 1.13. From it, the time variation of the deformation at any point x may be deduced.

The first disturbance would reach x in x/W_1 sec. and by x/W_2 sec. the unit deformation would be e_2. At any greater time t the deformation e at any x is

$$(e)_x = e_2 + \frac{(e_3 - e_2)(W_2 t - x)}{(W_2 - W_3)t} \tag{1.110}$$

or in ratios,

$$(e/e_2)_x = 1 + \frac{(e_3/e_2 - 1)\left[\dfrac{W_2 t}{L} - \dfrac{x}{L}\right]}{(1 - W_3/W_2)W_2 t/L} \tag{1.111}$$

where $\dfrac{x}{L}$ is the location of the strain gage and $\dfrac{W_2 t}{L}$, the location of e_2 along the bar, is a measure of elapsed time.

The curves of Fig. 1.14, calculated from Eq. 1.111 for strain gages at $x/L = .05$ and $x/L = .30$ differ from observed curves. The calculated slip deformation builds up more rapidly than is observed in tests. This indicates that the straight line deformation distribution of Fig. 1.13 is not as likely as the dotted curve indicated. This means that attributing a linear average value of stress energy and kinetic energy to the material in the slip zone gives results that are too high. This would imply that the values of elastic deformation e_2 calculated from such a "lump constant" analysis should turn out to be a bit low since the energy left behind in the slip zone appears to have been over estimated.
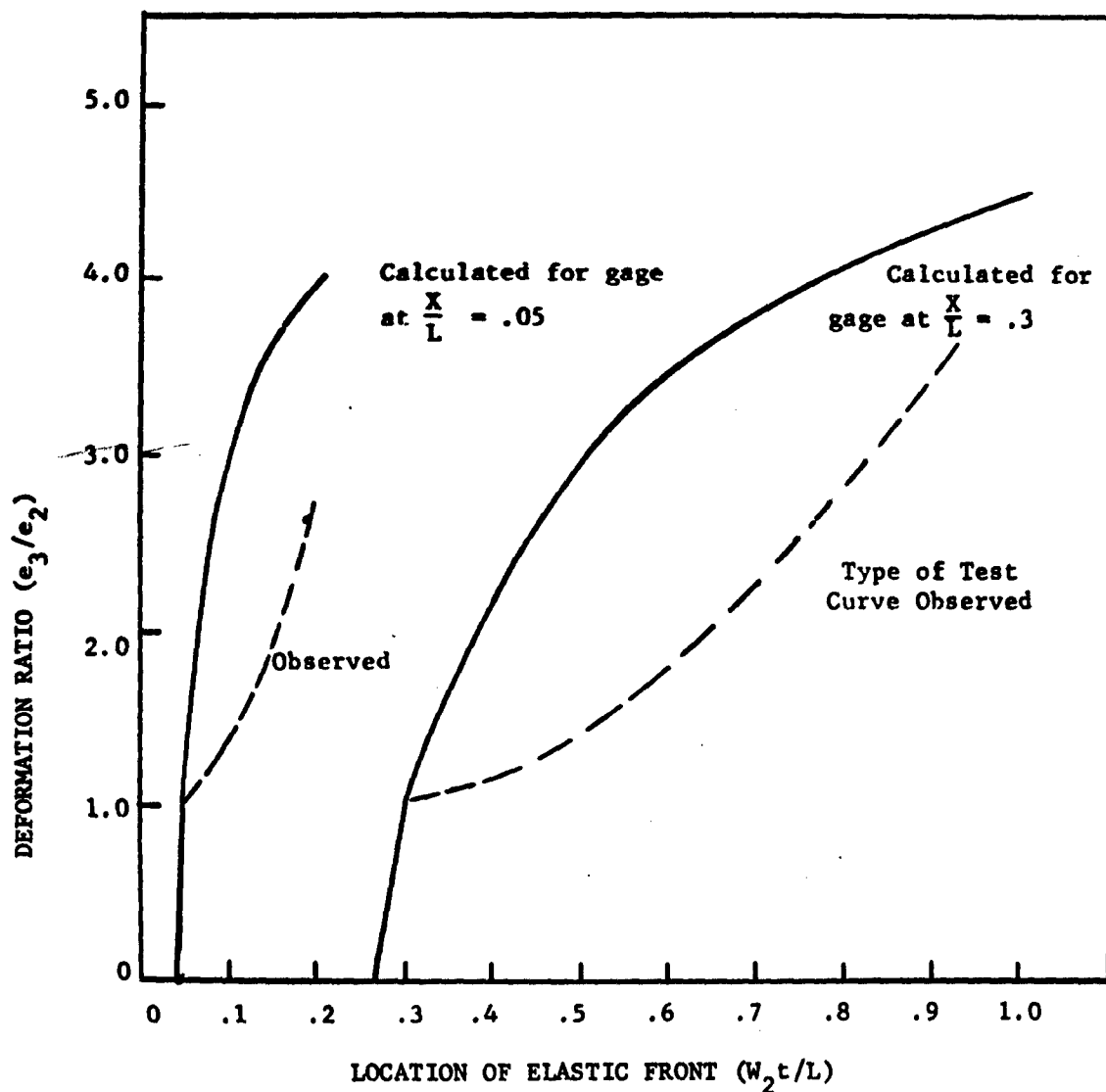
-- 37 --

Fig. 1.14. Deformation ratio $\dfrac{e_3}{e_2}$ versus location of elastic

front $W_2 t/L$. Calculated curves are compared

with the observed curves for the following assumed

conditions: $\dfrac{W_1}{W_2} = 1.1$, $\dfrac{e_3}{e_2} = \dfrac{\text{slip deformation}}{\text{elastic deformation}} = 5.0$

and $\dfrac{W_3}{W_2} = .2$ for one gage at $X/L = 0.0t$ and one

at $X/L = 0.3$.

- 38 -

1.11 Comparison of Analysis and Tests

Since the elastic deformation e_2, Fig. 1.9, can be determined reasonably well from strain gage traces, this deformation e_2 is shown for steel, aluminum, and copper in Figs. 1.15, 1.17, and 1.19. The theoretical curves were calculated from Eqs. 1.75, 1.74, and 1.76 using the properties of Table 1.1 and from values of u_3, $\dfrac{S_3}{E_2}$, and $\dfrac{u_3}{S_3 e_3}$ taken from Figs. 1.2, 1.2a, 1.3, 1.3a, 1.4, and 1.4a.

Values of $u_3/S_3 e_3$ and $E_2 e_3/S_3$ in Eq. 1.75 yield values of e_2 and Eq. 1.74 gives corresponding values of impact velocity V_3 needed to produce such deformations. The velocity W_3 of the back of the slip zone was calculated from Eq. 1.76. For the linear range of the stress-strain curves 1.2, 1.3, and 1.4, $e_3 = e_2$, there is no slip and $V_3 = e_2\sqrt{E_2/\rho}$. This linear portion of the e_2 vs. V_3 curve is shown extended on Figs. 1.15, 1.17, and 1.19. Figures 1.16, 1.18, and 1.20 show the corresponding values of e_2 and W_3 plotted against the total slip deformation e_3.

As would be expected from Fig. 1.14, it was at times difficult to know where e_2 ended and the effects of the slip deformation e_3 began, particularly for strain gage locations near the impact end of the bar. As was shown by Eq. 1.109, the velocity V_3 of Figs. 1.15, 1.17, and 1.19 is 1/2 of the velocity V_o of the shot rod.

Three things stand out in this comparison of test results with analytical predictions:

1. Particularly for aluminum, there appears to be distinct evidence of an elastic wave with no apparent slip at deformations greater than that of the elastic limit of the static stress-strain curve.
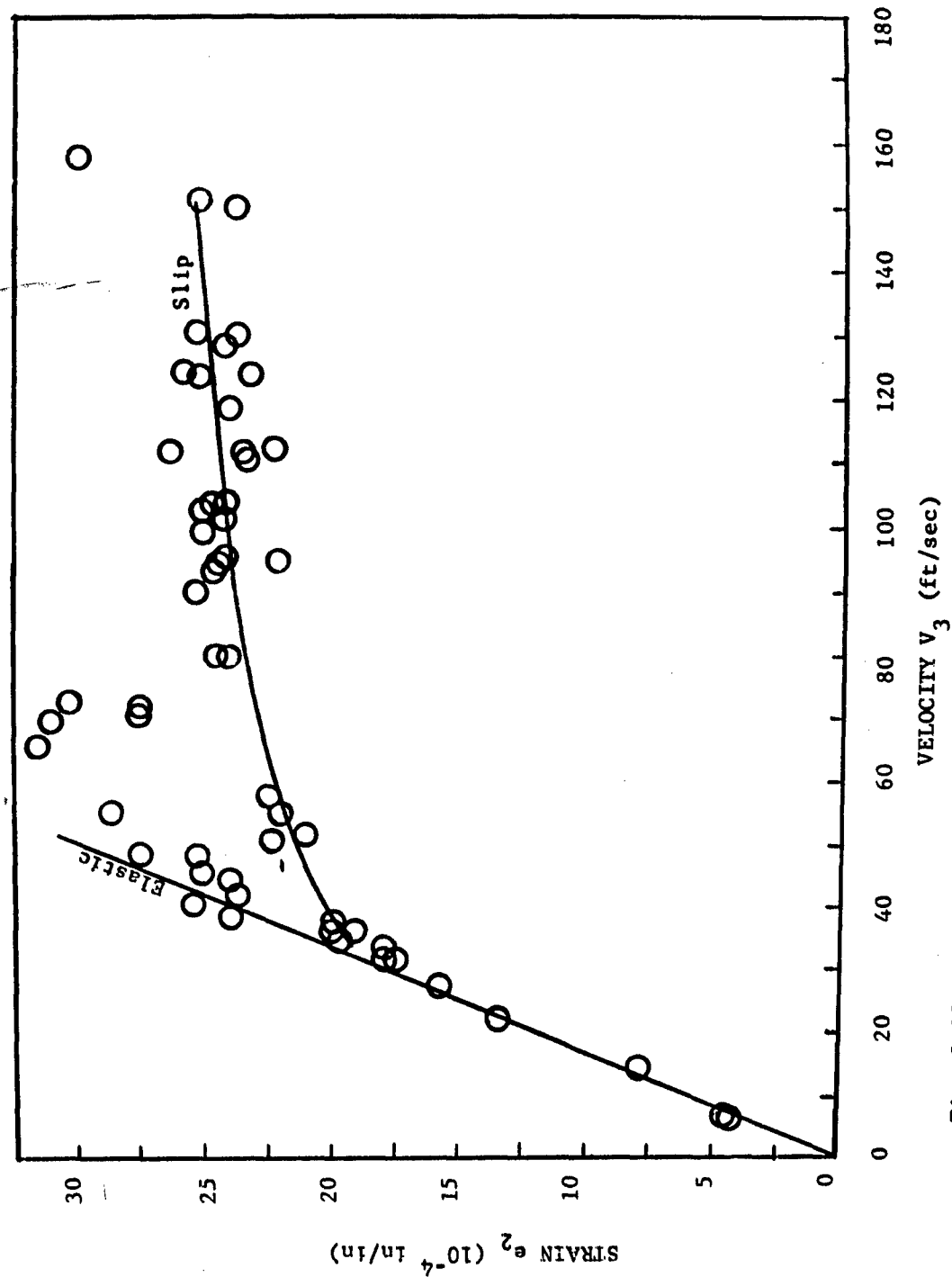
Fig. 1.15. Strain e_2 plotted against velocity V_3 comparing the theoretical curve with the experimental results for 1018 steel.
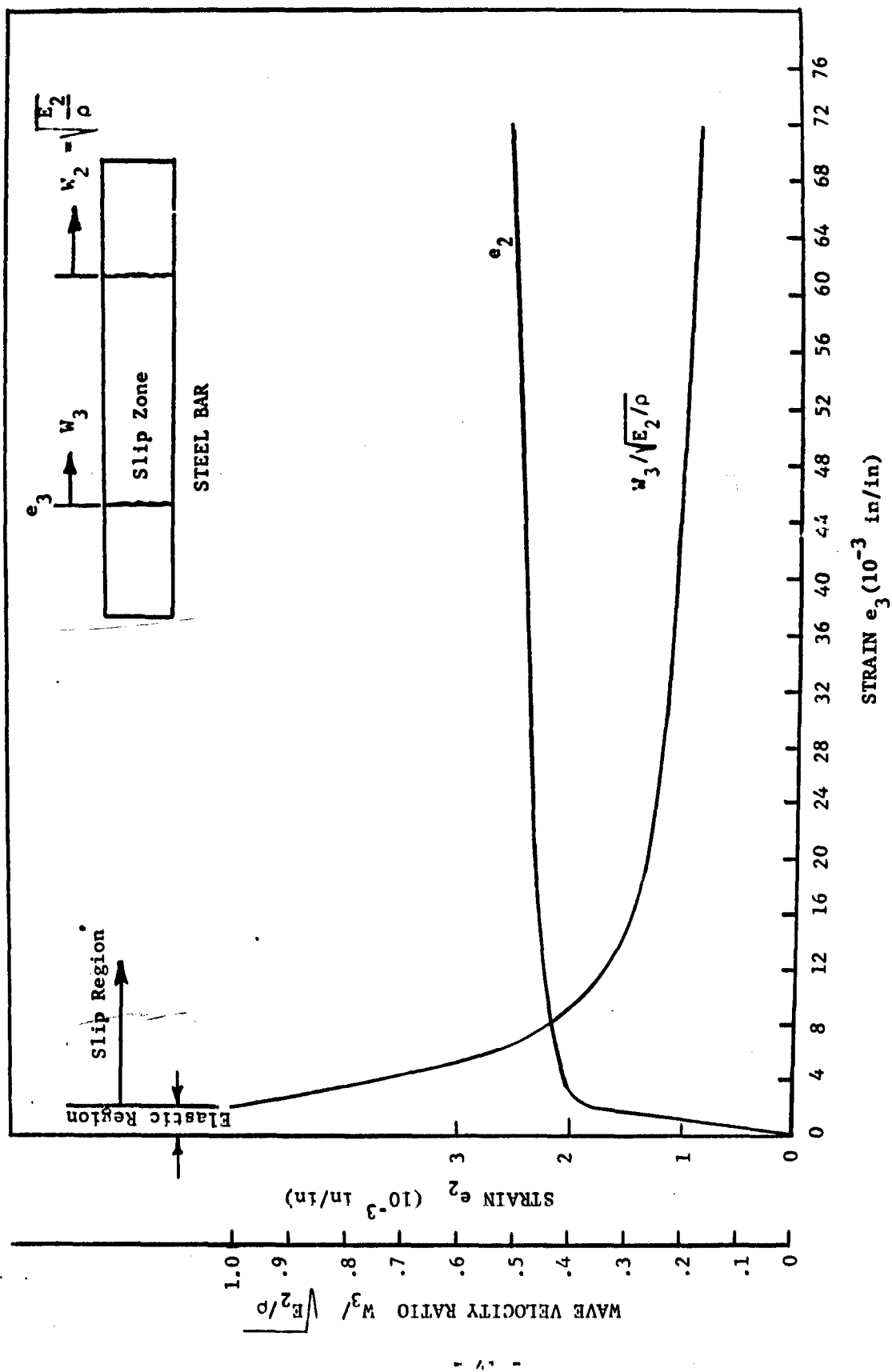
Fig. 1.16. Strain e_2 and wave velocity ratio $W_3/\sqrt{E_2/\rho}$ plotted against strain e_3 for 1018 steel. (Theoretical calculations).
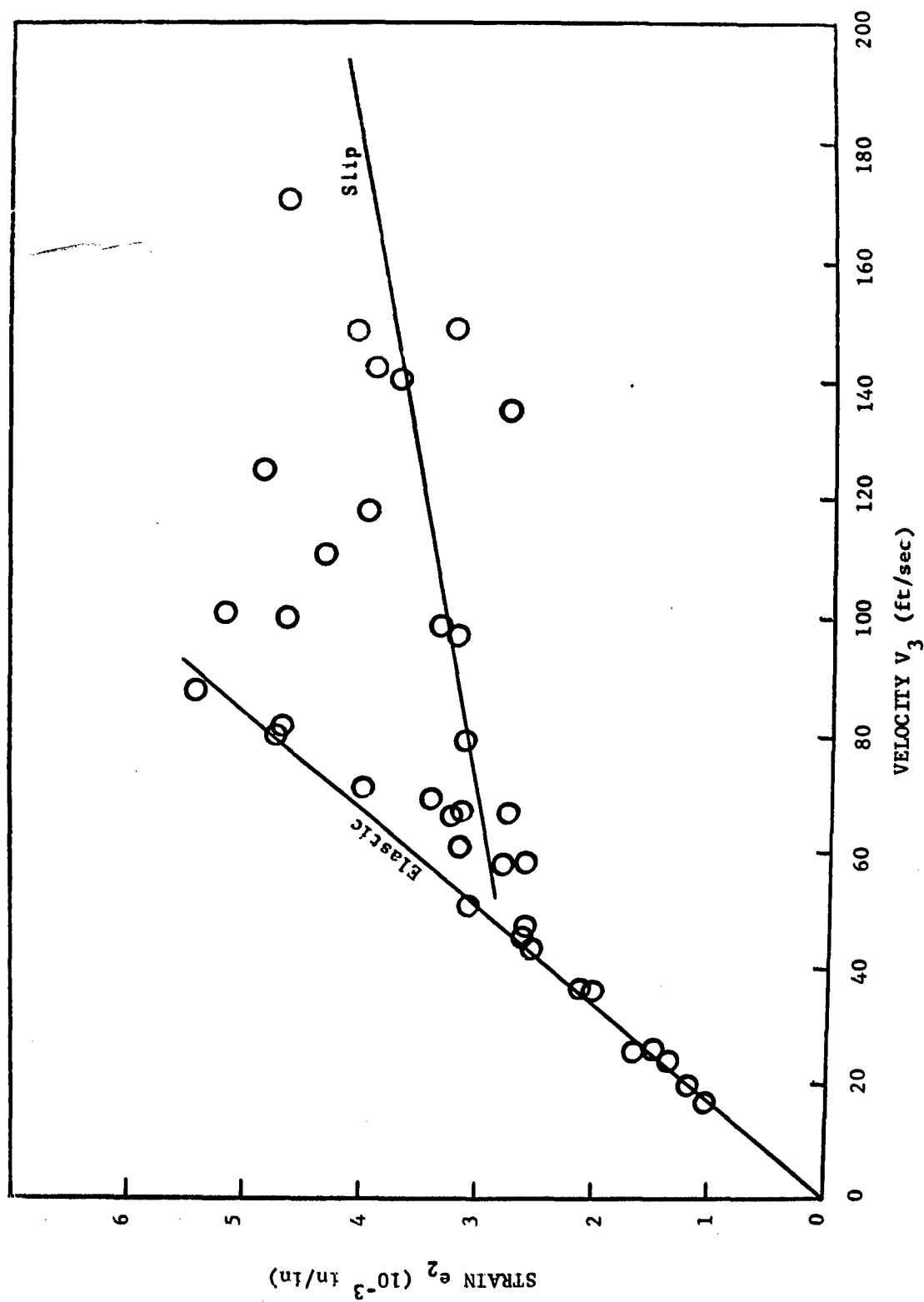
Fig. 1.17. Curve of strain e_3 in/in against velocity V_3 ft/sec comparing the experimental results with the theoretical calculations for 24T4 aluminum.
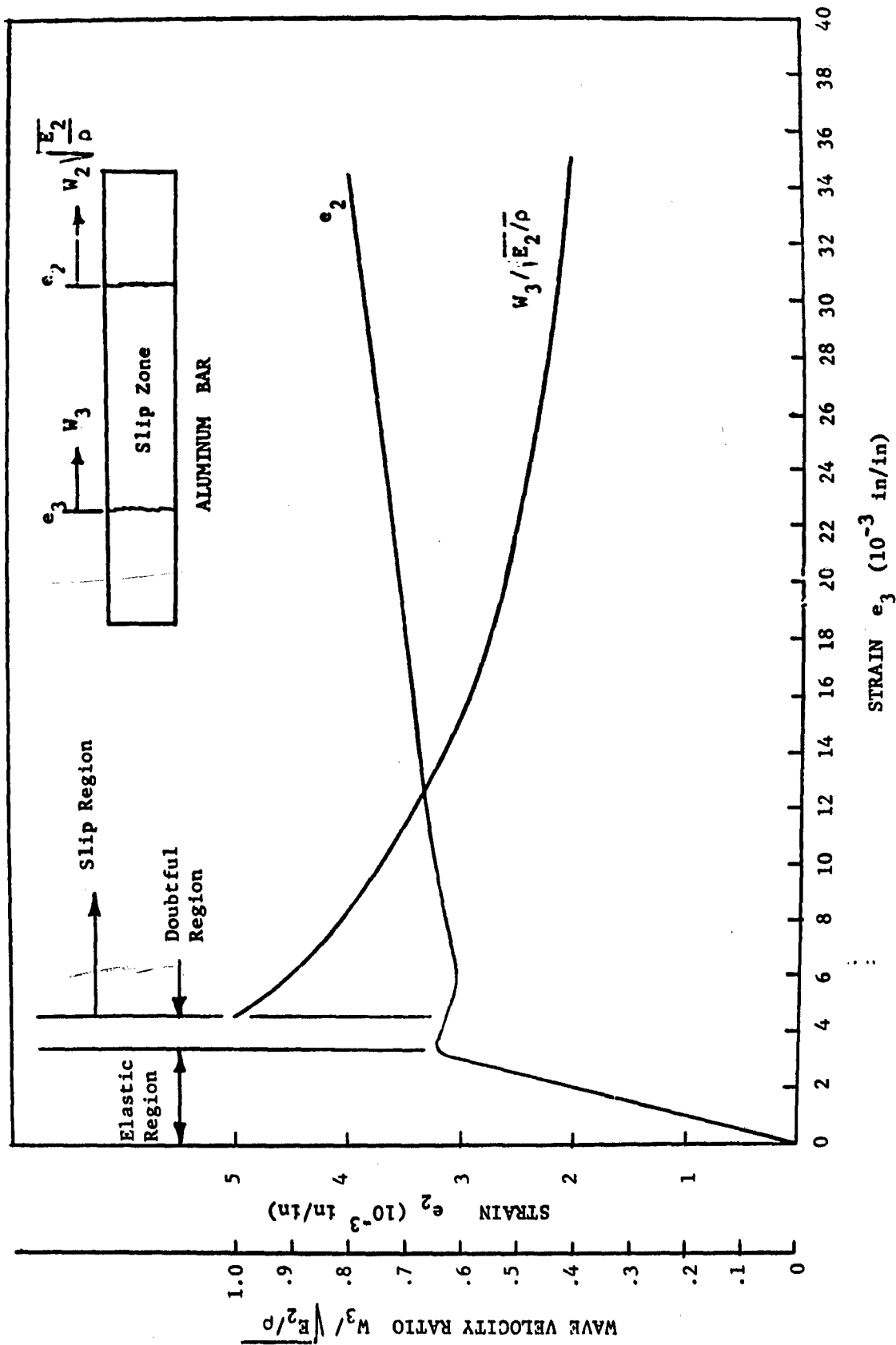
Fig. 1.18. Curves of strain e_3 against strain e_2 and the wave velocity ratio $W_3 / \sqrt{E_2/\rho}$ for 24T4 aluminum.
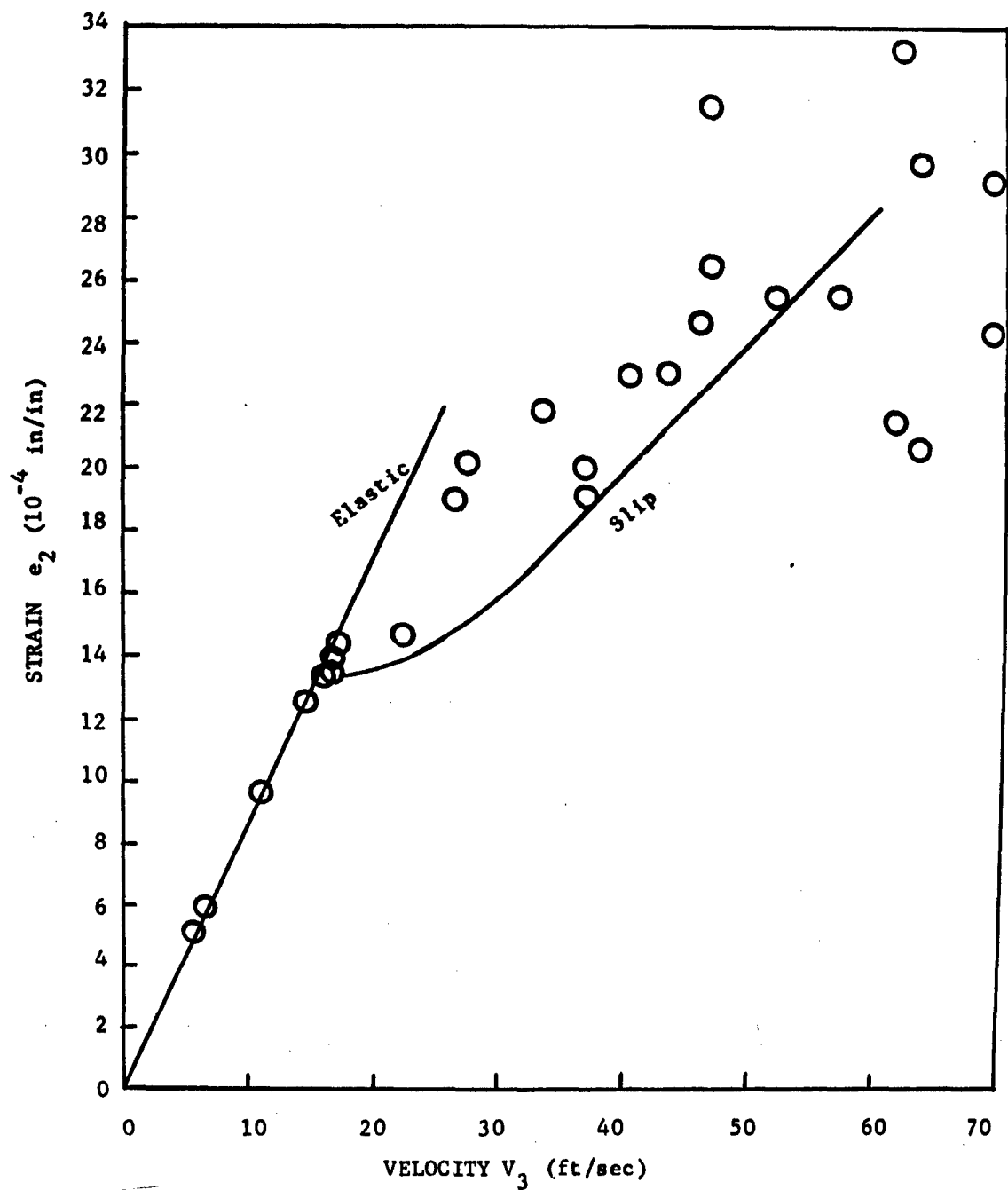
Fig. 1.19. Graph of strain e_2 versus velocity V_3 comparing the experimental data with the theoretical curve for copper.
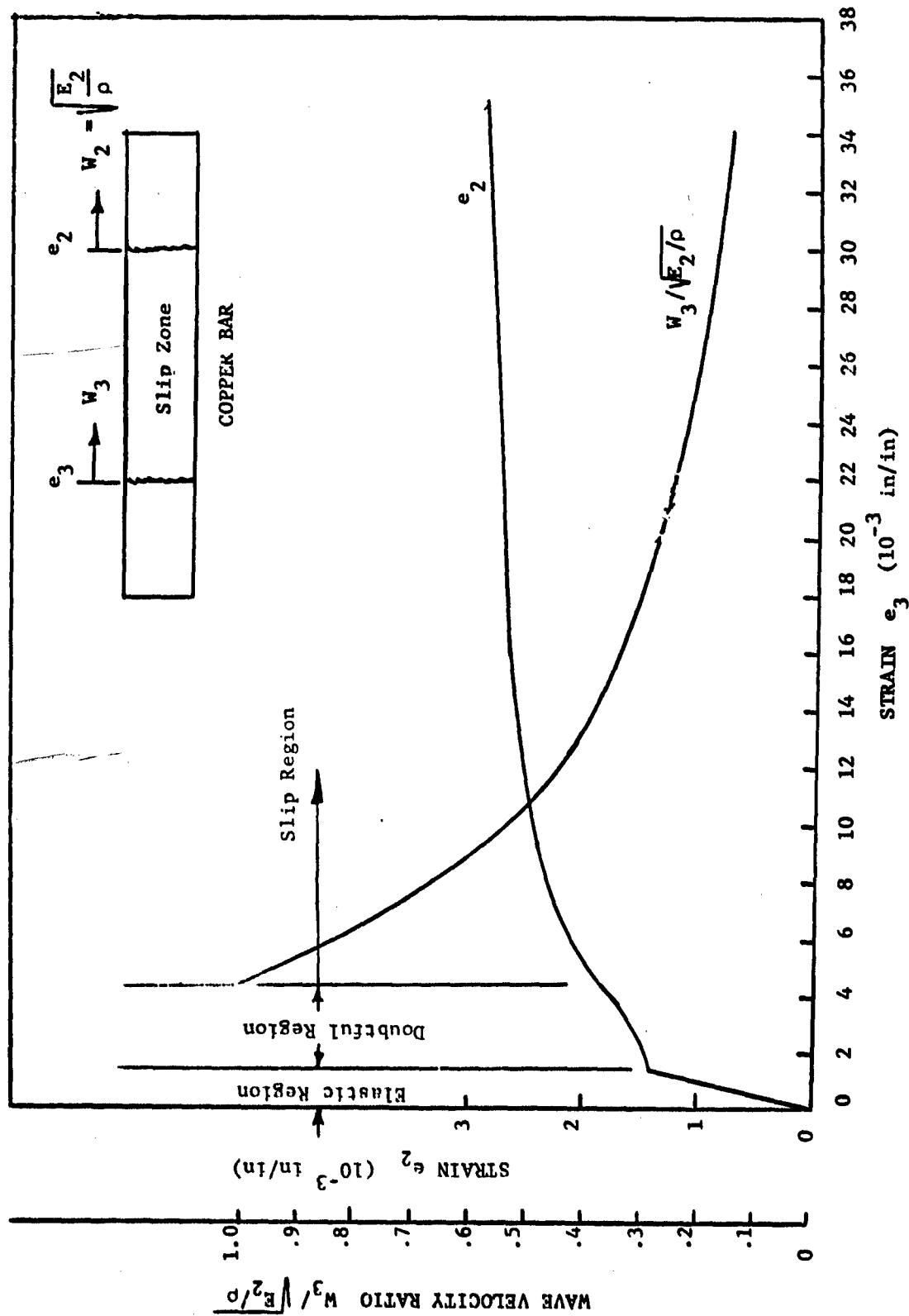
Fig. 1.20. Curves of strain e_3 against strain e_2 and the wave velocity ratio $W_3/\sqrt{E_2/\rho}$ for copper.

2. While there is considerable experimental uncertainty in the experimental evaluation of the deformation e_2, the consistency of the trends supports the concept of elastic waves and slip zones upon which the analysis was errected.

3. Figures 1.16, 1.18, and 1.20 indicate that while the slip deformation e_3 increases rapidly with the striking velocity V_3, the deformation e_2 of the elastic front increases but slightly. It is quite significant that the velocity W_3 of the back of the slip zone decreases rapidly as the severity of the impact increases. This directly affects the ability of energy to escape into the material at the point of impact and thereby increases the local damage resulting from the impact.

II. EQUIPMENT AND TESTING

2.1 Static Compression Tests

Static compression tests were made on 3/4" diameter by 2" long specimens of 1018 steel, 24T4 aluminum, and copper. The tests were conducted with a 60,000 pound capacity Olsen testing machine and a microformer strain-load recorder (a drum stylist type recorder). A specimen was loaded to a certain stress and then relieved with the load and strain being recorded during both the stressing and relieving periods. A new specimen was used for each different load to eliminate work hardening effects. Strain gages were also used simultaneously to check the strain and stresses in the elastic region with those indicated by the recorder. These tests were run because of the lack of suitable compression data for these materials and also because the dynamic tests were to be performed under fast compression loading. These data were used in the development of the theory of the dynamic part of the experiment. The actual stress strain curves of 1018 steel, 24T4 aluminum, and copper are shown in Figs. 1.2, 1.3, and 1.4 respectively.

It is definitely seen from the recorded information that the recovered energy for any applied load is always less than the input energy. This is true even in the elastic region. Thus some permanent strain is always present and the slope of the recovery line is always steeper than the previous loading line. Stated otherwise, the recovery modulus of elasticity is always greater than the loading modulus of elasticity. Figure 1.1 illustrates this phenomena.

2.2 Dynamic Test Apparatus

A special gun consisting of one solid section, a breech solenoid section, and a barrel extension alignment section was designed, fabricated, and used to accelerate the metal rods. It has a smooth bore of 0.500 inches in diameter and is chambered to fire a 50 caliber cartridge. The gun is mounted on two steel blocks whose design allows motion in the axial as well as the transverse direction for alignment purposes. The mountings are bolted in place to a stationary metal table which holds the entire test set up, and the table is rigidly fastened to the wall of the concrete tunnel in which the tests have been conducted. An air gun was also developed by adapting a gas solenoid valve to the already existing gun barrel and it is used for low rod velocities. Photographs of the powder gun and air gun are shown in Figs. 2.1 and 2.2 respectively. A schematic diagram of the complete test set up is shown in Fig. 2.3.

2.3 Test Rods

Twelve inch long rods of 1018 steel, 24T4 aluminum, and copper were machined to as close to 0.499 inches in diameter as possible. The ends were machined and all machine marks were removed with an aluminum oxide cloth. This was done in order to reduce to a minimum any concentrated local stresses which might be set up upon impact. Of every pair of rods machine, one rod was to be accelerated in the previously mentioned 50 caliber gun while the other was to be used as a stationary rod instrumented with strain gages at various locations. The back end of each stationary rod was placed firmly against a hardened and rigidly fastened 4340 steel surface so that little or no deformation of the rod at that location would exist, thus creating a
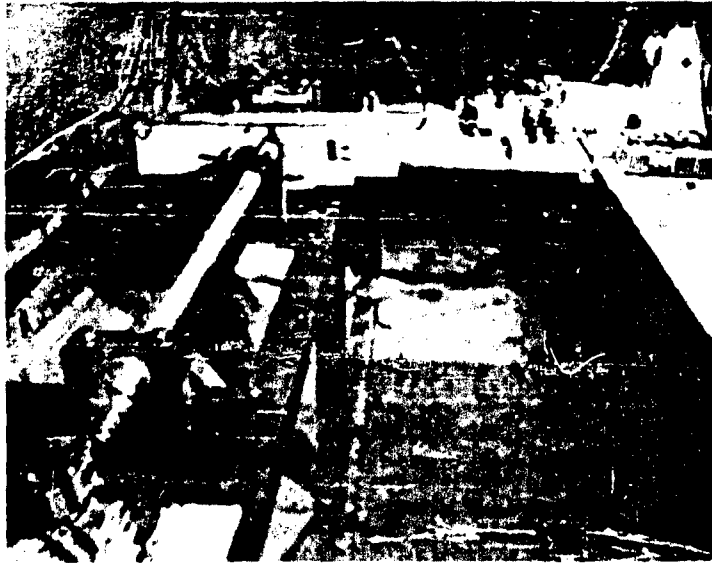
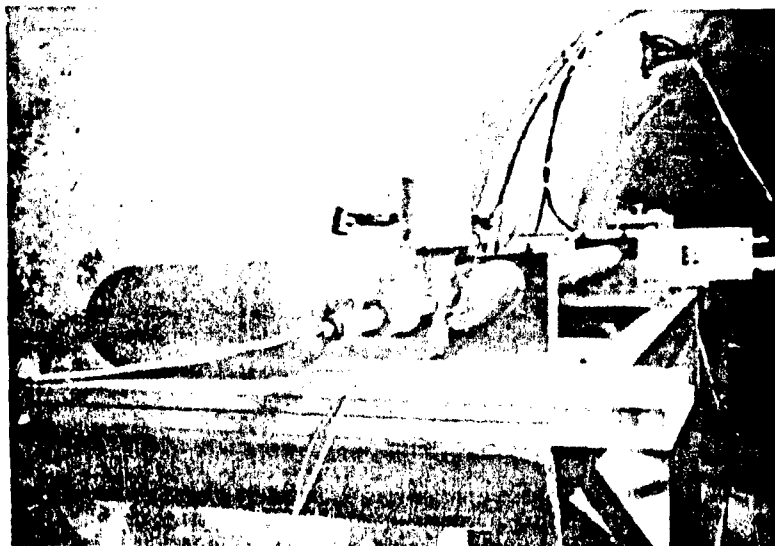Fig. 2.1.   Photograph of power gun used
            to accelerate test rods.

Fig. 2.2.   Photograph of air gun used to
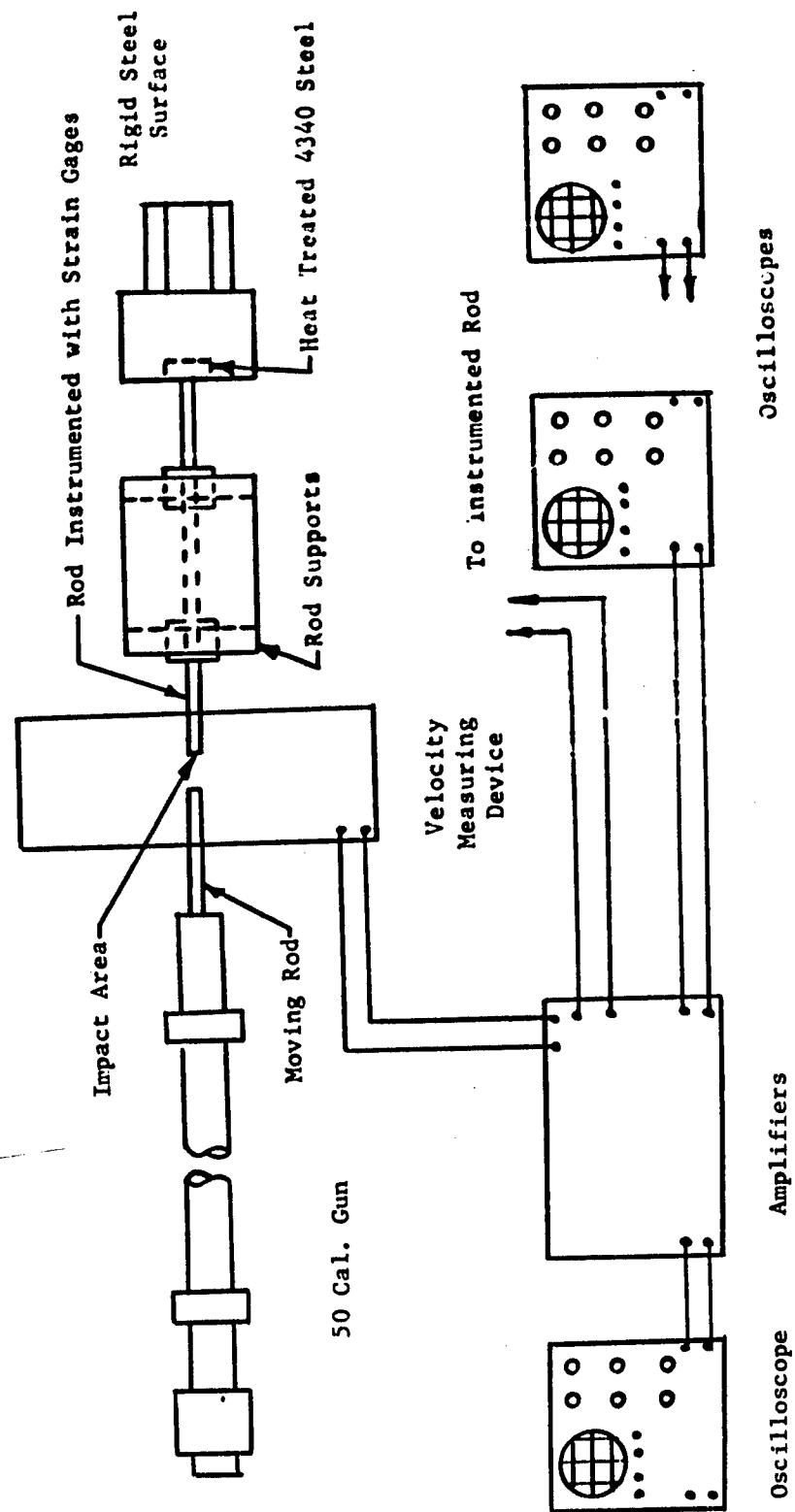   accelerate test rods.

- 49 -

Fig. 2.3. Schematic Diagram of Test Setup.

fixed end condition. The dimension of 12 inches for each rod insured length enough to measure the propagated velocity of the wave front with considerable precision. Also, because about 5 inches of the moving rod was still in the gun barrel upon impact, good alignment was maintained. The impact and stationary rods were aligned before each firing so as to impact squarely and uniformly.

The 12 inch long metal rods were first fired into a box of sand without impacting with other rods so as to determine either the mass of powder or air pressure (depending upon which gun was used) required to produce the subsequent desired velocities. The velocity measuring system developed and utilized is discussed in a later section of this report. Velocities as high as 1700 ft/sec were measured, but it was later found out that from 10 ft/sec to 500 ft/sec was the most practical range in which to work and record good data. Graphs of powder load against rod velocity and air pressure against rod velocity are shown for steel only in Figs. 2.4 and 2.5 respectively. These curves were used only to predict the mass of gun powder or air pressure needed to produce a desired velocity for the velocity was measured on each firing.

2.4 Dynamic Strain Measurements

Budd and SR-4 strain gages, designed especially for dynamic loading conditions, were placed at various locations on the stationary rod. Each strain gage was wired into a separate amplifier designed specifically for the strain gages and then connected directly to one or more oscilloscopes. The amplifiers and strain gages are discussed in Section 3 of this report. The vertical scale of the oscilloscope in volts per centimeter was converted
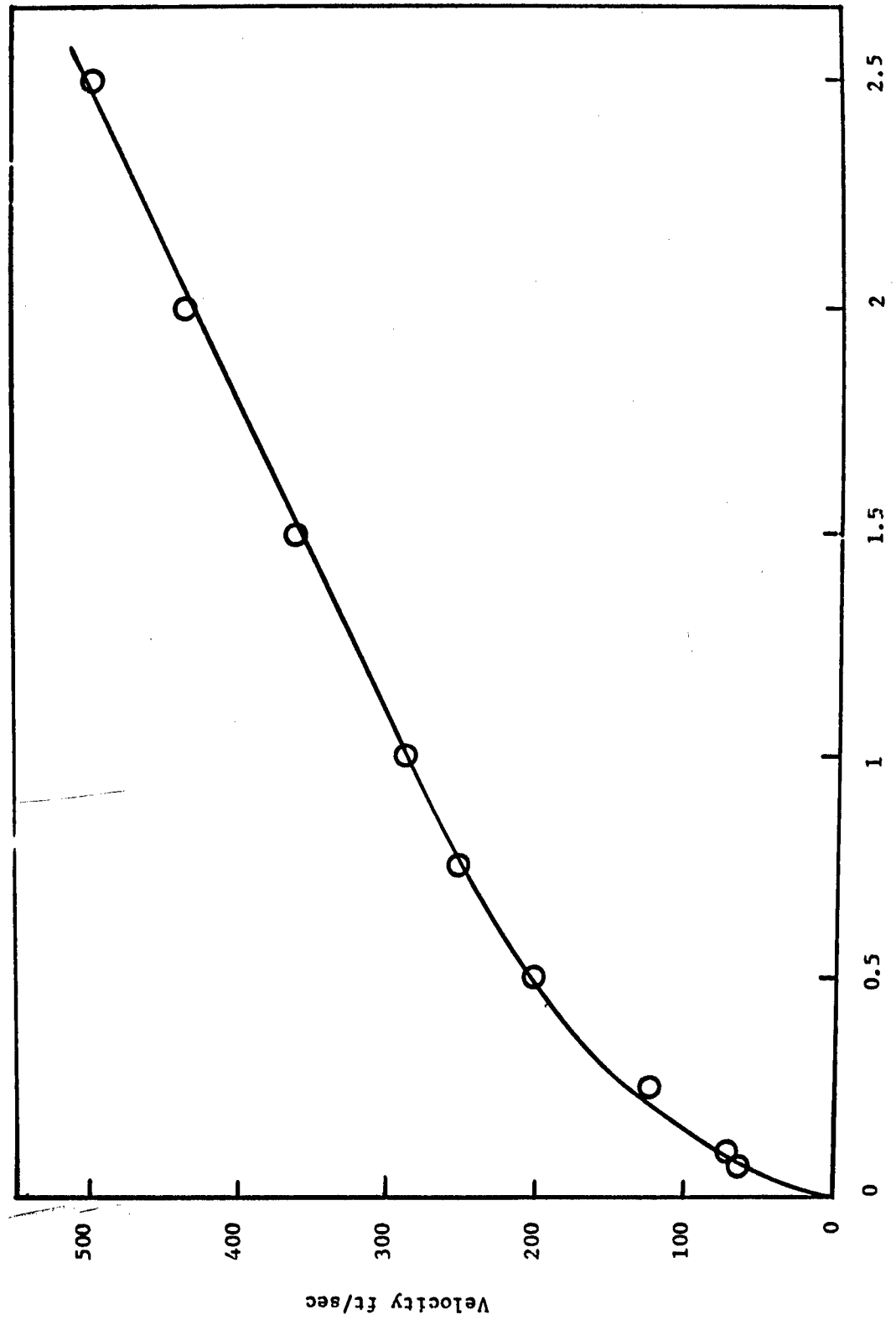
Fig. 2.4. Graph displaying velocity of 1/2 inch diameter 12 inch long 1018 steel rod and the mass Hercules 4064 powder.
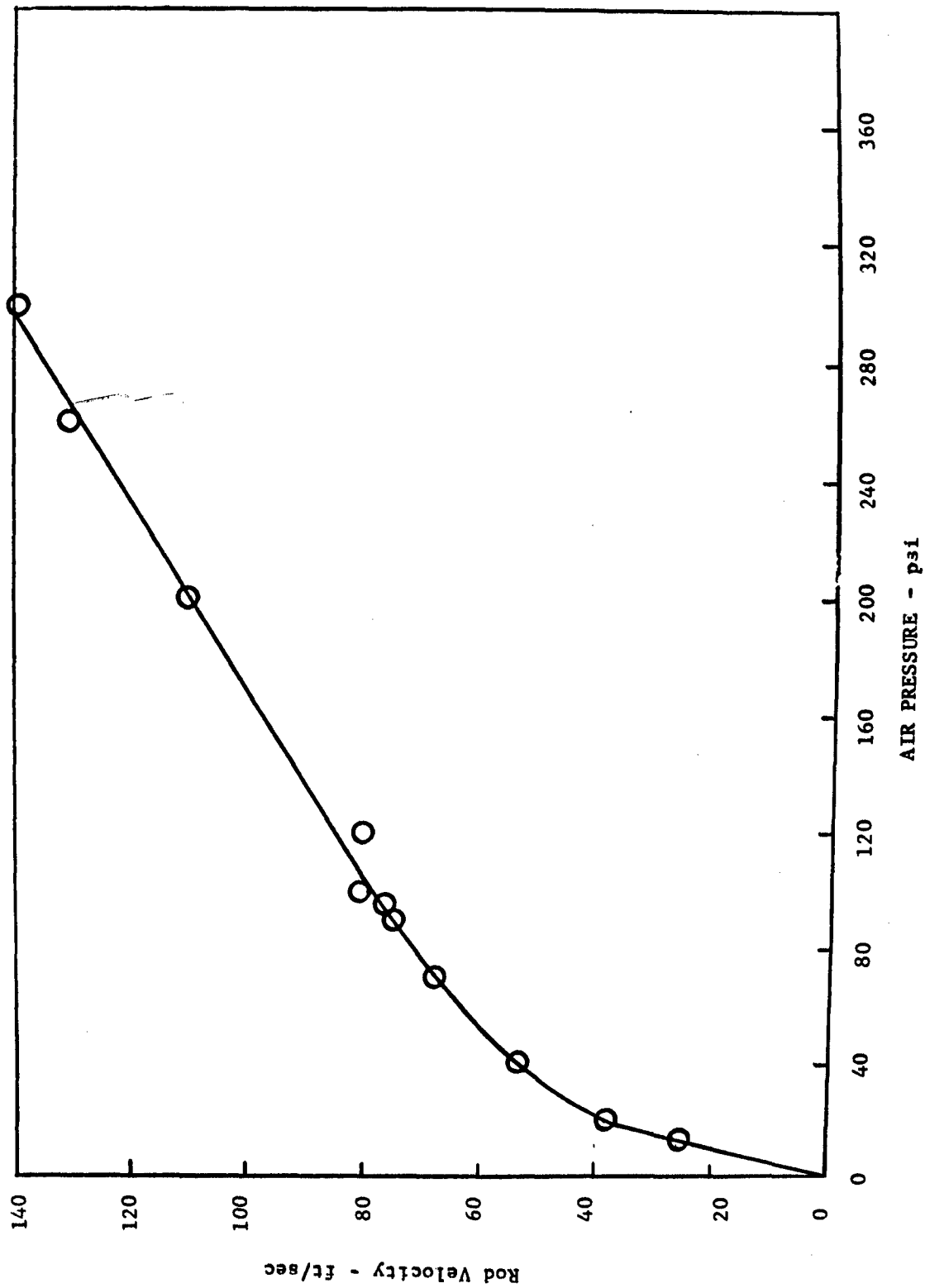
Grams of Hercules 4064 Powder

Velocity ft/sec

Fig. 2.5. Graph displaying rod velocity versus air pressure for 1/2" diameter × 12" long 1018 steel rod.

to inches per inch strain per every centimeter through an equation developed for each amplifier and which is also discussed in Section 3. Therefore, the photographs taken by the cameras attached to the oscilloscopes were essentially of strain versus time. Sketches of some of the types of photographs taken are illustrated in Figs. 2.6 and 2.8. The strain labeled e_2 in a previous discussion is actually the vertical deflection of the almost vertical part of the trace shown in Fig. 2.8a. A different e_2 was indicated and measured for each different impact velocity. This experimental data of one half the rod impact velocity versus strain e_2 can be seen in Figs. 1.15, 1.17, and 1.19 for 1018 steel, 24T4 aluminum, and copper respectively, and there compared with the theoretical curves. The actual data from which the experimental curves were constructed appear in tables A.1, A.2, and A.3 of the Appendix for steel, aluminum, and copper respectively.

The wave velocity W_1 was measured by placing two strain gages on a rod a considerable known distance apart in the same plane of reference and observing the time in micro seconds between which the front and back strain gages were first disturbed. The average of the wave velocities for all three materials are reported in Table 1.1. The wave velocity W_1 was found experimentally to be independent of how hard the bar was struck and thus, for any particular material, constant for all impact velocities.

One interesting observation made which further strengthens the theory previously discussed is the fact that a strain very close to the impact end displayed almost a vertical elastic front, whereas the slope continued to decrease for strain gages placed farther away from the impact end. This indicates strongly, as mentioned in Section 1.7 that because W_1 travels faster than W_2 the distance between them becomes greater as they move

- 54 -

down the rod, and the rise time for the elastic wave front or zone is increased. This is illustrated in Fig. 2.6.
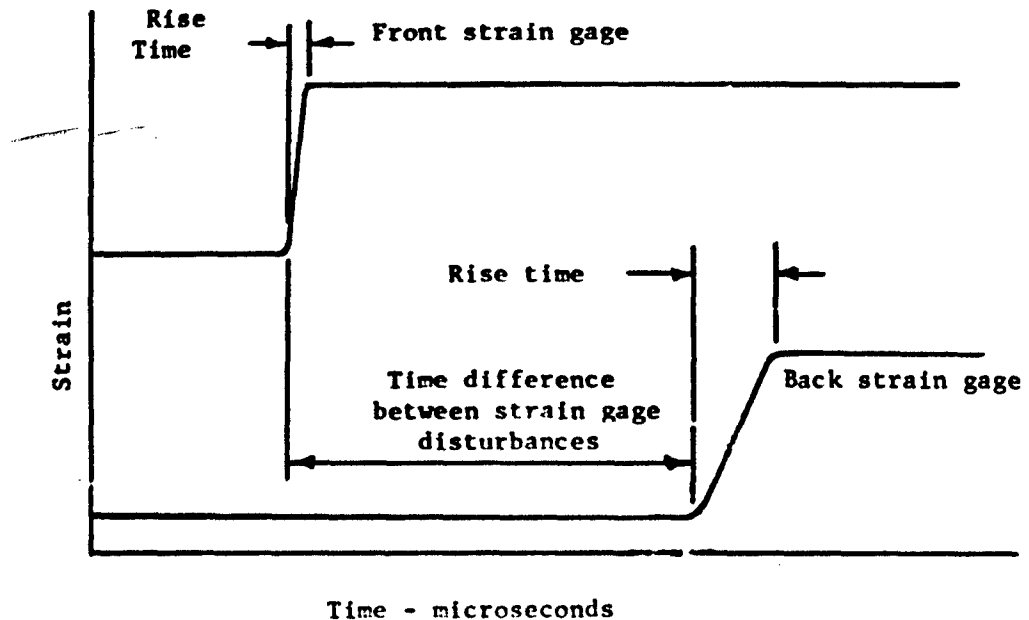

Fig. 2.6. Sketch displaying rise time of wave
           front versus strain gage position.

Because W_1 and W_2 are constant values for a particular material, theory predicts the rise time of the elastic slip zone to be linearly increasing with distance. A graph displaying the theoretical rise time versus distance is shown in Fig. 2.7 and there compared with some experimental values for 1018 steel only.

One other item that should be mentioned concerns that of recognizing the correct strain gage output voltage which, after being amplified, was photographed as it appeared on an oscilloscope. This voltage value was
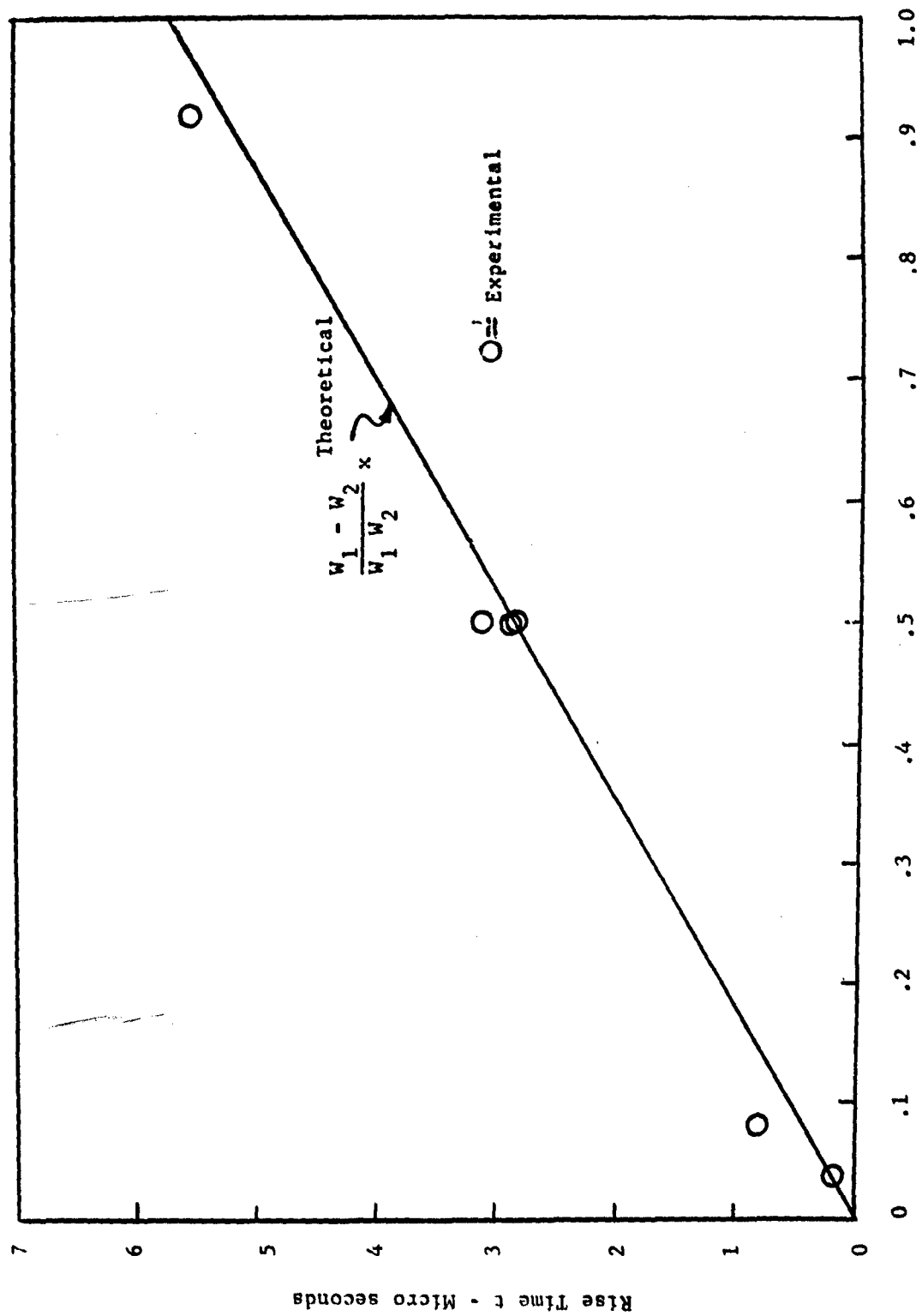
- 55 -

Fig. 2.7. Graph displaying rise time versus distance along rod for 1018 steel only.

used directly in the calculation of strain as is discussed in Section 3 of this report. Three different types of photographs of the accumulated data which required careful judgment to decipher are shown in Fig. 2.8. One type that was not so difficult to interpret is that of Fig. 2.6.
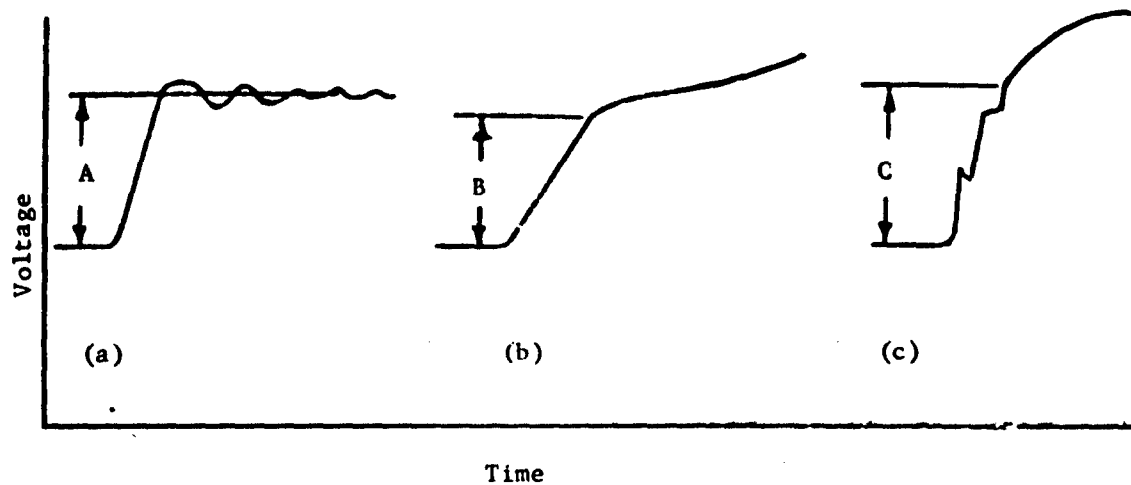

Fig. 2.8. Sketch displaying different type photographs taken of the strain gage output.

For the type of photograph illustrated in Fig. 2.8a, the distance A was taken to be the correct voltage value because it represented an average strain of the material processed by the wave front W_2. For the type of photograph illustrated in Figs. 2.8b and 2.8c, distances B and C were taken to be the correct voltages simply because they represent the linear range of the strains. Other types of photographs taken presented little or no difficulty to decipher.

Finally, of the two kinds of gages used, the SR-4 strain gage generally indicated strain values which fell very close to the theoretical curves as compared to the Budd strain gages whose strain indications fell further

- 57 -

away. So far, no explanation for this difference has been found, and all data taken from both gages are displayed. The majority of the SR-4 gages were used on steel and very few on copper and aluminum; therefore, the experimental points which appear very near the theoretical curves are more abundant on the steel curve than on the others.

3. INSTRUMENTATION

3.1 Deformation Measurements

3.1.1 Strain Transducers

Recent literature has shown that a number of methods have been used to measure deformations in materials.[1,2,3,4] Of these methods the strain-gage technique appears to be the simplest, cheapest, and the least time consuming and was therefore adopted for this project. The strain gage instrumentation is somewhat simplified in this case since most of the phenomena to be measured occur within 200 microseconds after the rod impact. For such an application, it is not necessary to use temperature compensated strain gages or dummy gages, a single gage attached to the rod at the desired spot and in the desired orientation being sufficient to provide strain measurements.

Figure 3.1 shows the strain gage circuit used with both the SR-4 and the Budd type strain gages.[*] The characteristics of these gages are also given in the figure. Both the SR-4 and the Budd gages are of the iso-elastic type, the former being a wire gage, the latter an etched foil gage.

---

[1] Walsh, J. M., Rice, M. H., McQueen, R. C., and Yarger, F. L., *Physical Review*, Vol. 108, p. 196, Oct. 1957.

[2] Bell, J. F., *Journal of Applied Physics*, Vol. 27, No. 10, p. 1109, Oct. 1956.

[3] Curtis, C. W., *Int. Symp. on Stress Wave Propagation in Materials*, Ed. by N. Davids, Interscience Publishers, New York, 1960, p. 15.

[4] Eichelberger, R. J., *Int. Symp. on Stress Wave Propagation in Materials*, Ed. by N. Davids, Interscience Publishers, New York, 1960, p. 15.

[*] Strain gages used were Budd, type 321-160, obtained from Budd Company, P. O. Box 245, Phoenixville, Pa., and SR-4 type C-11 obtained from Baldwin-Lima-Hamilton Corp., Electronics and Instrumentation Div., Waltham, Mass.
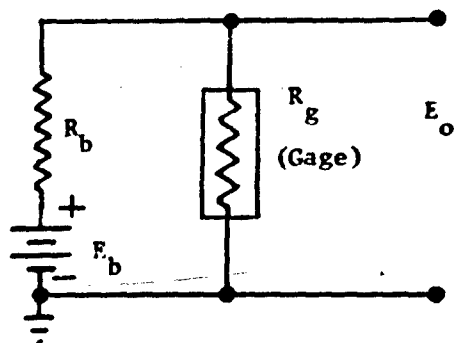
	SR-4	Budd
Type	C-11	321-160
R_g	300 ± 2	$160 \pm .2$ ohms
Gage Factor	$2.86 \pm 2\%$	$2.98 \pm 1\%$
R_b	100 ± 1	100 ± 1 ohms
E_b	12	6 volts (approx.)
Active Gage size	1/8 x 1/8	1/8 x 1/8 inches

Fig. 3.1. Strain-Gage Circuit for Use with
SR-4 and Budd Gages.

These gages were chosen because of their small size, high gage factor, and availability. SR-4 gages can be fastened in place by simply gluing the gage to the test rod with either Duco or SR-4 solvent-type cement. These cements require approximately 12 hours drying time before use. The Budd gages must be fastened on with an epoxy-type cement such as Budd GA5 epoxy adhesive. This epoxy needs an elevated temperature for proper curing, a typical curing rate being 200° F. for one hour.

The output of the strain-gage circuit of Fig. 3.1 can be calculated as a voltage which is directly proportional to the strain on the gage. The output voltage E_o is

$$E_o = E_b \left(\frac{R_g}{R_b + R_g} \right) \qquad (3.1)$$

If R_g changes by ΔR_g, then E_o changes by ΔE_o so the output is

$$E_o + \Delta E_o = E_b \left(\frac{R_g + \Delta R_g}{R_b + R_g + \Delta R_g} \right) \qquad (3.2)$$

Solving for ΔE_o

$$\Delta E_o = E_b \left[\frac{R_g + \Delta R_g}{R_g + R_b + \Delta R_g} - E_o \right] = E_b \left[\frac{R_g + \Delta R_g}{R_b + R_g + \Delta R_g} - \frac{R_g}{R_b + R_g} \right] \quad (3.3)$$

Letting $a = \dfrac{R_b}{R_g}$, ΔE_o becomes

$$\Delta E_o = E_b \ \frac{a}{1+a} \left[\frac{\Delta R_g}{R_g} \right] \left[\frac{1}{1 + a + \dfrac{\Delta R_g}{R_g}} \right] \quad (3.4)$$

If $\dfrac{\Delta R_g}{R_g}$ is small compared to $1 + a$, ΔE_o can be approximated by

$$\Delta E_o = \frac{E_b a}{(1 + a)^2} \ \frac{\Delta R_g}{R_g} \quad (3.5)$$

The gain factor, G.F. is defined as

$$G.F. = \frac{\dfrac{\Delta R_g}{R_g}}{\dfrac{\Delta L}{L}} \quad (3.6)$$

Where $\dfrac{\Delta L}{L}$ is the strain on the gage. Combining Eqs. 3.5 and 3.6 gives

$$\frac{\Delta L}{L} = \frac{(1 + a)^2}{a} \ \frac{\Delta E_o}{E_b \ G.F.} \quad (3.7)$$

For SR-4 strain gages (type C-11)

$$\frac{\Delta L}{L} = 1.87 \ \frac{\Delta E_o}{E_b} \quad (3.8)$$

For Budd gages (type 321-160)

$$\frac{\Delta L}{L} = 1.42 \ \frac{\Delta E_o}{E_b} \quad (3.9)$$

3.2 Amplification, Matching, and Recording

A block diagram of the firing tunnels and control consol is shown in Fig. 3.2. As shown, the output of each strain gage circuit is carried to an oscilloscope through an amplifier, a cathode-follower, and a terminated co-axial cable. Channels 4, 5, 6, and 7 are identical in construction and nearly identical electrically, differing only slightly in their gains. The overall gain of each channel is tabulated in Fig. 3.2. This gain represents the voltage gain between the input to the amplifier and the output at the end of the terminated co-axial cable. The complete circuit diagram for one of these channels is shown in Fig. 3.3.

The velocity with which an elastic wave travels down a steel rod is approximately 17,000 feet per second. Assuming the elastic wave to have a very sharp front, it will then take approximately .6 microseconds for this wave front to pass beneath a strain gage whose axial length is 1/8 of an inch. For this reason the strain gage amplifiers are designed to have a rise time of 0.1 microsecond. Figure 3.4a is a photograph showing a rise time of .3 μsecs. which is typical of channels 4, 5, 6, and 7. This response time is that of the complete system including the strain gage amplifier, cathode-follower, co-axial cable, termination, and oscilloscope.

The output of the strain gages during a test is photographed directly from the oscilloscope using Polaroid Land cameras. A typical photograph of strain gage outputs in shown in Fig. 3.4b. All strain gage channels may be used simultaneously. For purposes of identification, the strain gage amplifier channels are numbered channels 4, 5, 6, and 7.

3.3 Velocity Measurements

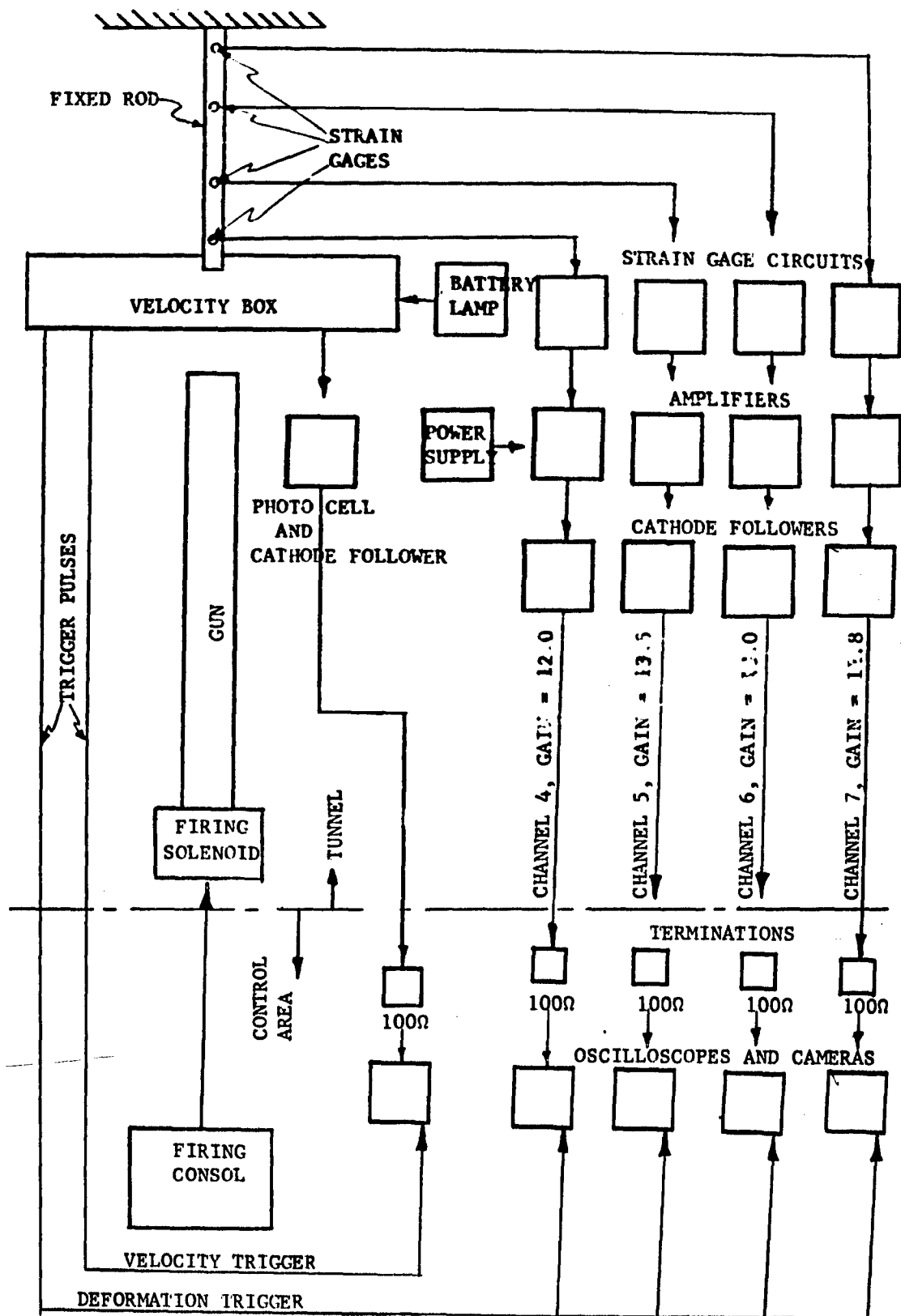The velocity of the rod as it approaches impact with the fixed rod must

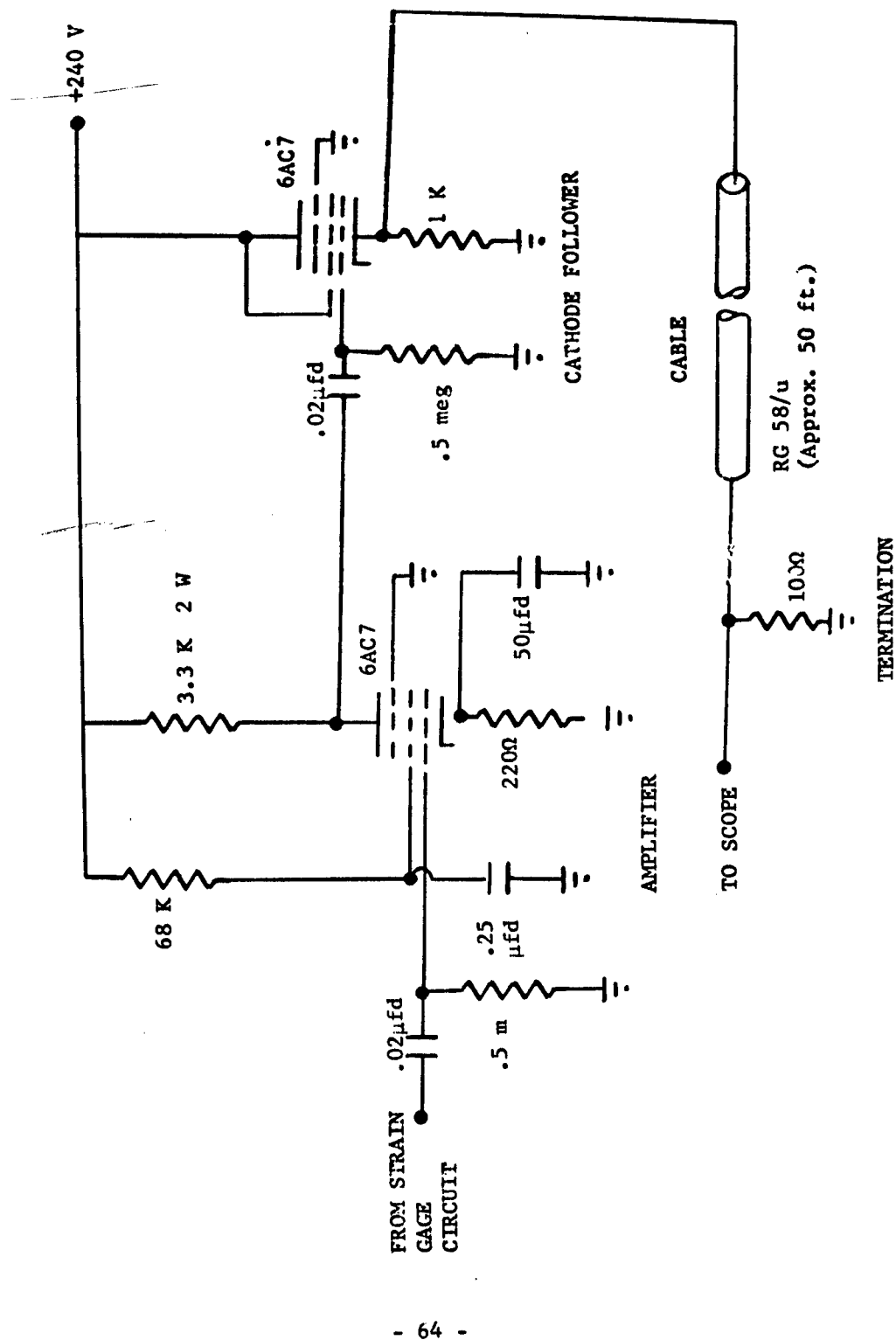**Fig. 3.2.** BLOCK DIAGRAM OF COMPLETE SYSTEM

Fig. 3.3. CIRCUIT DIAGRAM FOR CHANNEL 4. CHANNELS 5, 6, AND 7 HAVE THE SAME DIAGRAM BUT DIFFER SLIGHTLY IN PHYSICAL ARRANGEMENT AND GAIN
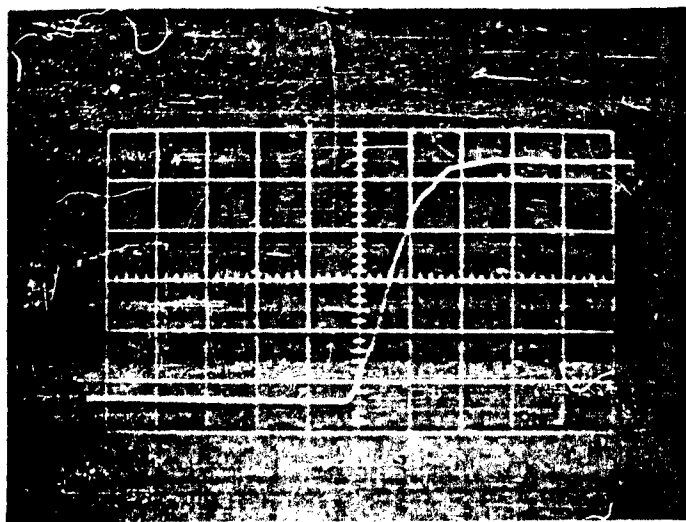
Fig. 3.4a.   Rise time for Channel 7.
             Sweep time - .2 μsec/cm
             Amplitude - .5 volts/cm
             Input to amplifier - 100 Kc square wave
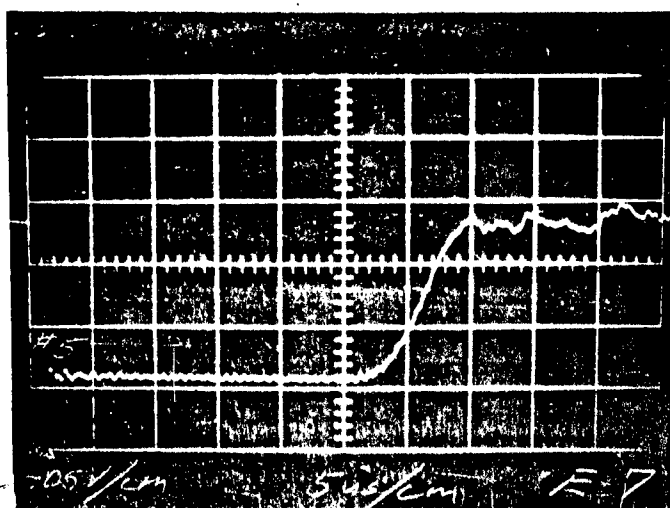   with rise and decay time less than
             .03 μsec.

Fig. 3.4b.   Typical Strain Gage Output.

be measured. In many experiments, the velocity of the projectile can be measured by allowing it to pierce two separate grids, spaced a fixed distance apart. The time necessary for the projectile to travel from one grid to the other can be precisely measured and the velocity calculated. Such a method, however, is not desirable when a precision impact is necessary, especially when using rods with accurately machined ends. It is possible that fragments of the grid may be carried ahead of the traveling rod. Such fragmentary pieces, depending on the material used for the gird, may cause distortions in the impact.

The velocity measuring device to be described here is an optical device eliminating the possibility of any grid fragments distorting the impact and also removing the possibility of any external applied forces on the rod as it moves toward the impact. Figure 3.5 is a simplified drawing of this system. Light from the lamp is collected by lens A and sent parallel through the elongated slit. The fixed rod is positioned such that the impact end of it interrupts a slight amount of the light at the impact end of the slit. The narrow beam of light is then collected by lens B and focused on a photo cell. The output of the photo cell is fed through a cathode follower and along a matched cable directly to an oscilloscope. As the traveling rod leaves the gun and moves toward the impact end of the fixed rod, it interrupts more and more of the narrow beam of light. The output of the photo cell begins to drop as soon as the traveling rod enters the light beam and continues to drop linearly as the traveling rod approaches the impact end of the fixed rod. After impact occurs, there is no further change in the photo cell output as long as the two rods stay together. If after some length of time the traveling rod bounces back out again, this will be indicated by an increasing voltage at

- 66 -

BACK UP
BLOCK

LENS B:

EY 516 (Eastman) f 5.0
12" Focal Point
Diameter 2 3/8"
Focal point 10 3/4"
from rear edge.

PHOTO CELL

LENS B

BAFFLE

SLIT

MOVING
ROD

LENS A

LAMP - 12 VOLTS
10 WATTS

GUN

LENS A:

EE 1494, f 2.5
7" Focal Point
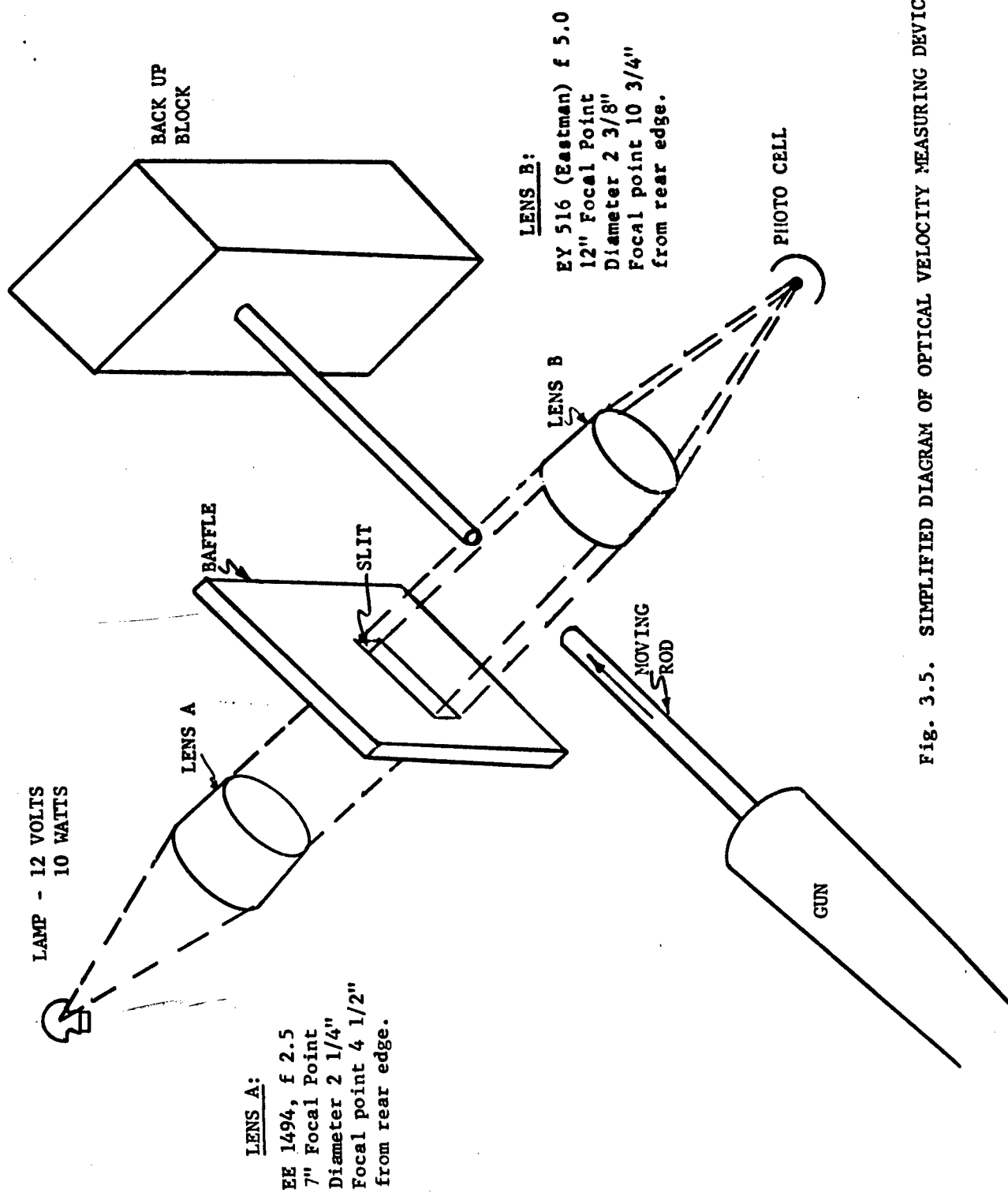Diameter 2 1/4"
Focal point 4 1/2"
from rear edge.

Fig. 3.5. SIMPLIFIED DIAGRAM OF OPTICAL VELOCITY MEASURING DEVICE

the photo cell output. From a photograph of the photo cell output as recorded on an oscilloscope, the time necessary for the moving rod to interrupt the light beam can be measured. This time, and the measured width of the beam being interrupted (d in Fig. 3.5), gives the average velocity of the rod just prior to impact. It is also possible to determine how long the two bars are in direct contact with each other and the nature of any bounce that may take place. A more detailed drawing of the velocity box is shown in Fig. 3.6.

The cathode follower associated with the photo cell is mounted inside the box immediately beside the photo cell. The photo cell circuit is shown in Fig. 3.7. A standard 12 volt automobile battery is used to power the 12 volt 10 watt automobile globe used as a light source. Half-inch plexiglass windows are provided on either side of the impact area to protect the lenses. The unit is placed near enough the end of the gun such that impact is achieved before the traveling rod completely leaves the gun. In this way, the moving rod is held firmly in place and a more accurate impact can be obtained. A typical velocity picture for a steel-to-steel impact at medium velocities is shown in Fig. 3.8.
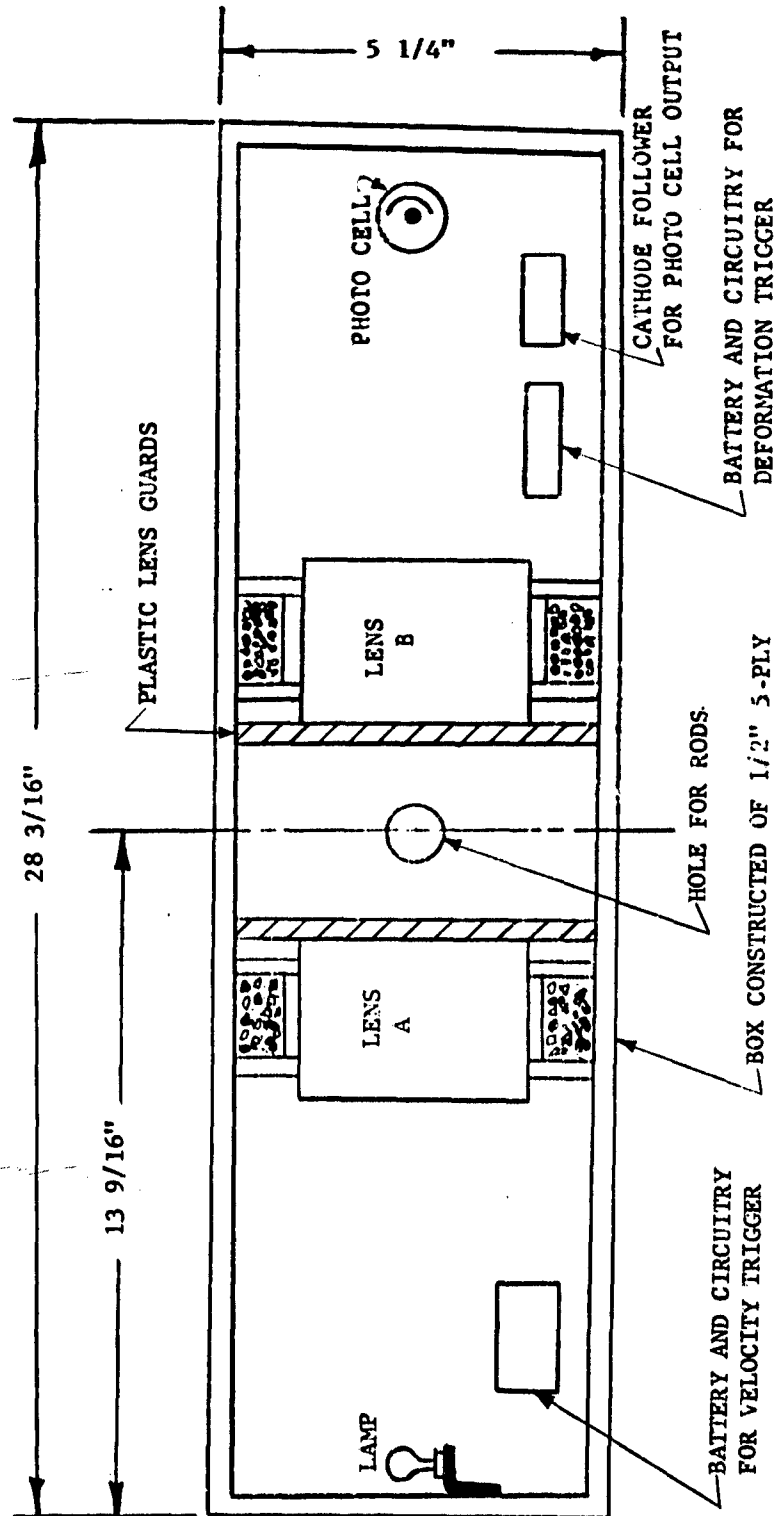
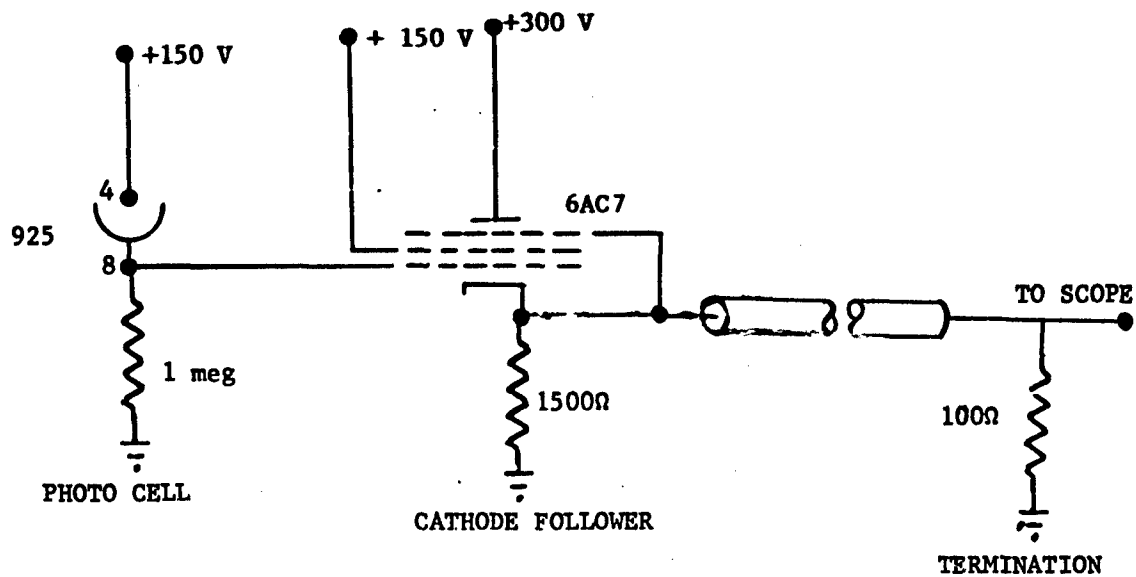Fig. 3.6. SIDE VIEW CROSS SECTION OF THE VELOCITY MEASURING BOX

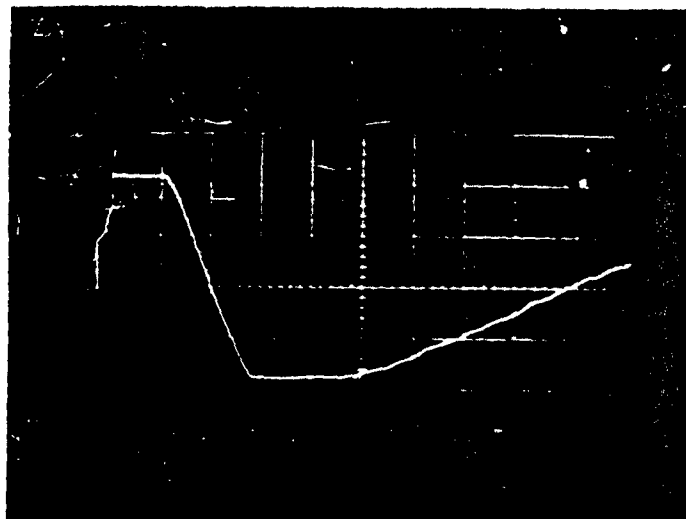Fig. 3.7. PHOTO CELL AND CATHODE FOLLOWER CIRCUIT DIAGRAM

Fig. 3.8. Velocity trace for steel-to-steel impact
          showing some bounce. Sweep .5 m sec/cm.,
          amplitude .2 v/cm, d = 2.21", t = .85 m sec.
          velocity = 217 ft/sec.

3.4 Trigger Circuits

3.41 Deformation Trigger

The trigger signal used to start the sweep circuit on those oscilloscopes
displaying the deformation voltages is generated at the time of impact. The
method used to obtain this trigger signal can best be explained by referring
to Fig. 3.9. As shown, the gun barrel is completely insulated from ground
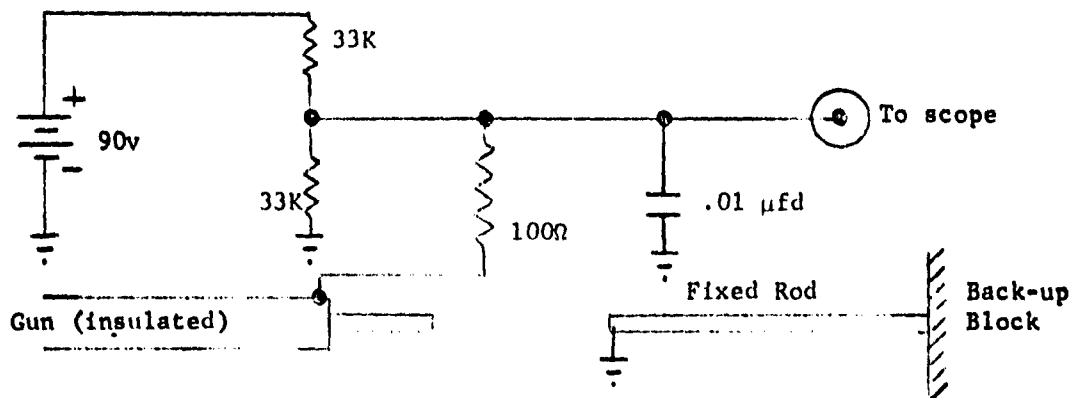
Fig. 3.9. Deformation trigger circuit.

- 71 -

and is initially at a potential of approximately 45 volts as determined by the resistor voltage divider. The 0.01 microfarad capacitor is also charged to 45 volts. The fixed rod is grounded as near to the impact end as possible. At the time of impact, the traveling rod is still in the gun and therefore when it hits the fixed rod, the gun is grounded. The capacitor then discharges with a theoretical time constant of 1 microsecond. However, due to small inherent inductances in the system, some overshoot is present. The oscilloscopes are adjusted to trigger as soon as the voltage drops by approximately 20 volts. Triggering is reliable within approximately one half of a microsecond and as many as five oscilloscopes can be triggered simultaneously with this system.

3.42 The Velocity Trigger

A separate trigger circuit is necessary to provide a signal to start the sweep on the velocity oscilloscope at some time just previous to the instant the traveling rod enters the light beam. This is accomplished by stretching a very fine cotton thread across the hole in the velocity measuring box through which the traveling rod enters. This cotton string is in turn attached to a number 34 copper wire which forms a part of the trigger circuit as shown in Fig. 3.10.
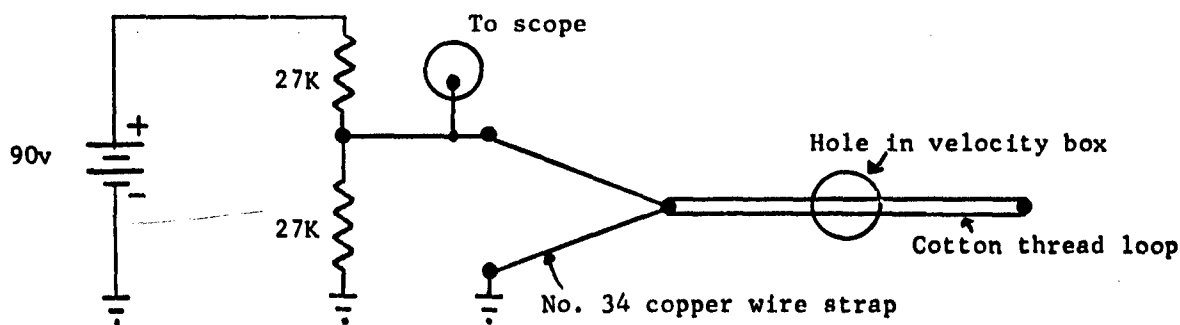
Fig. 3.10. Velocity Trigger Circuit

- 72 -

This small copper wire forms a short across one of the 27 K resistors forcing the trigger output to be at 0 potential. As the traveling rod enters the hole, it strikes the cotton cord which in turn breaks the number 34 wire strap. The output then immediately arises to approximately +45 volts, and the scope triggers. The cotton string is adjusted such that it breaks at the same time the copper wire breaks and no fragments are carried into the impact area.

In cases where only velocity measurements are being made, it is possible to place the copper wire strap directly over the hole itself eliminating the need for the cotton string. This cannot be done when deformation measurements are being made, however, because the copper strap is at ground potential and will give a premature deformation trigger signal at the instant the traveling rod hits and breaks the copper wire strap. For convenience, the trigger-circuit batteries and components are mounted inside the velocity measuring box in such a way as not to interfere with the light beam.

3.5 Accuracy of the Battery and Strain Gage Circuit

The gage resistance of a Budd strain gage is $160 \pm .2\Omega$. This gives an accuracy figure of $\pm 0.125\%$. The ballast resistor R_b of the strain gage circuit (See Fig. 3.1) is a 1% resistor. The battery voltage, being measured with a calibrated instrument, can be read with an accuracy of $\pm 1\%$. The change in the output voltage of the strain gage circuit of Fig. 3.1 is given by Eq. 3.4 which is repeated here.

$$\Delta E_o = E_b \; \frac{a}{1 + a} \left[\frac{\Delta R_g}{R_g} \right] \left[\frac{1}{1 + a + \frac{\Delta R_g}{R_g}} \right] \qquad (3.4)$$

where a has been defined as R_b/R_g. For the errors of R_b and R_g as given above,

the maximum error in a will be $\pm$ 1.125%. The term $\angle R_g/R_g$ has a maximum

percentage error of 0.25%. Of all of the terms in the denominator of the

quantity contained within the second set of brackets in Eq. 3.4, the term a

has the largest percentage error. Thus, the largest maximum error that can

occur in the sum of terms $1 + a + (\angle R_g/R_g)$ is 1.125%. Equation 3.4 can be

rewritten indicating the percentage error in each of the terms as shown in

Eq. 3.10.

$$\Delta E_o = E_b (\pm\ 1\%)(\frac{a}{1 + a})(\pm\ 2.25\%) \left[\frac{\angle R_g}{R_g}\ (\pm\ 0.25\%) \right] \left[\frac{1}{1 + a + \frac{\angle R_g}{R_g}}\ (\pm\ 1.125\%) \right] \quad (3.10)$$

This makes the net maximum error in the output voltage of the strain gage

circuit ΔE_o equal to about $\pm$ 4.63%.

3.51 Amplifier and Oscilloscope Calibration Accuracy

The gain of each amplifier was measured from the input to the amplifier

to the final scope termination and also included the oscilloscope amplifiers

themselves. An input wave was placed directly on the input of the amplifier

and also compared directly to the amplified wave on the oscilloscope. It

is estimated that the accuracy of this overall calibration is of the order

of $\pm$ 3%. This includes the amplifier, cable, cable termination, oscilloscope

amplifier and reading of the oscilloscope face. Since the output voltage

of the strain gage circuit must be multiplied by the amplifier gain to obtain

the total output, the errors of the two quantities must be added giving a

total overall maximum deviation of $\pm$ 7.25%. It should be pointed out, however,

that in each case we have taken the worst possible error. It is possible

that consistency in reading data and measuring distances on the oscilloscope face could decrease the maximum error by a factor of one-half or more, especially when the comparisons are to be made between a number of data points all taken on the same channel and in the same manner.

APPENDIX

Data for various curves are compiled in the Appendix and are identified with the particular curve by figure numbers.

TABLE A-1

1018 STEEL DATA
Fig. 1.15

Rod Velocity ft/sec	Strain in/in	Rod Velocity ft/sec	Strain in/in
12	.000426	116	.00224
14	.000445	131	.00316
29	.00080	141	.00275
43.5	.00135	143	.00275
53.4	.00157	145	.00291
63	.001795	160	.0024 .00245
63.1	.00176		
66	.0018	180	.00254
		186	.00246
68	.00198	188.5	.00245
72	.0019 .00201	190.5	.0022
75.5	.0020	191	.00242
76	.0024	198	.00251
76.7	.00238	202	.00246
79.5	.00256	203	.00240
83.5	.00237	205	.00243
88	.0024	206	.0025
90	.00251	207	.00246
95	.0027	208	.0024
95.5	.00275	220	.00232
96	.00254	223	.00234
101.5	.00223	224	.0022 .00264
104	.0023		
110	.00287 .00221		

TABLE A-1

1018 STEEL DATA
(continued)

Rod Velocity ft/sec	Strain in/in
237	.0024
247	.00252
248	.00231 .00259
256	.00243
261	.00253
270	.00237
299	.00237
301	.00252
317	.0030
418	.00251

Rod Velocity ft/sec	Strain in/in	Rod Velocity ft/sec	Strain in/in
34.5	.00105	175	.00542
40.3	.00119	193	.00315
48.3	.00138	197.2	.00332
52.6	.00148	197.5	.00462
53.5	.00175	201.5	.00515
72.5	.00204	221	.00433
74	.00218	236	.00396
87	.00254	249	.00485
92	.00261	259	.00275
96	.0026	281	.00366
100.8	.0031	285	.00422
			.00376
116	.00259	297	.00321
	.00278		.00407
120.7	.00318	340	.00467
131	.00314	525	.00415
132	.00324		
133	.00315		
	.00276		
138.5	.00341		
141.5	.00376		
158	.00311		
160	.00447		
163	.00442		

TABLE A-3
COPPER DATA
Fig. 1.19

Rod Velocity ft/sec	Strain in/in	Rod Velocity ft/sec	Strain in/in
10.7	.0051	126.3	.00298
			.00205
13.2	.0006		
		138	.00292
21.8	.000976		.00243
28.8	.00126	182	.00268
31.9	.00134	191	.00221
			.00321
32.9	.00135		
33.5	.0014		
33.7	.00145		
43.75	.00147		
52.5	.0019		
54.75	.00202		
66.2	.00219		
73.2	.00191		
	.00209		
79.6	.0023		
85.5	.00231		
86	.00231		
91	.00248		
91.8	.00316		
92.5	.00265		
103	.00255		
113	.00255		
122	.00216		
124.6	.00333		

AD-

University of Utah, High-Velocity Laboratory, Salt Lake City, Utah HYPER-ELASTIC IMPACTS by Neil P. Bailey, C. E. McDermott, D. K. Gehmlich, and E. P. Palmer. May 1962. 80 p. illus. tables. (Technical Report UU-8; AFBMD-TR-62-)
Unclassified Report

A study was made of one-dimensional wave propagation in and above the

(over)

UNCLASSIFIED

1. Wave Propagation Theory, Measurements

2. Linear and non-linear materials

I. Bailey, N. P. McDermott, C.E. Gehmlich, D. K. Palmer, E. P.

UNCLASSIFIED

AD-

UNCLASSIFIED

elastic range in rods of 24T4 aluminum, 1018 steel, and copper. Theory was developed describing the waves as consisting of a front of decreasing steepness followed by a zone of inelastic slip. Strain gage measurements were used to verify the theory.

II. Air Force Ballistic Missile Division, Air Research and Development Command

III. Contract AF 04(647)-942

UNCLASSIFIED

AD-

UNCLASSIFIED

elastic range in rods of 24T4 aluminum, 1018 steel, and copper. Theory was developed describing the waves as consisting of a front of decreasing steepness followed by a zone of inelastic slip. Strain gage measurements were used to verify the theory.

II. Air Force Ballistic Missile Division, Air Research and Development Command

III. Contract AF 04(647)-942

UNCLASSIFIED

AD-

UNCLASSIFIED

elastic range in rods of 24T4 aluminum, 1018 steel, and copper. Theory was developed describing the waves as consisting of a front of decreasing steepness followed by a zone of inelastic slip. Strain gage measurements were used to verify the theory.

II. Air Force Ballistic Missile Division, Air Research and Development Command

III. Contract AF 04(647)-942

UNCLASSIFIED

AD-

UNCLASSIFIED

elastic range in rods of 24T4 aluminum, 1018 steel, and copper. Theory was developed describing the waves as consisting of a front of decreasing steepness followed by a zone of inelastic slip. Strain gage measurements were used to verify the theory.

II. Air Force Ballistic Missile Division, Air Research and Development Command

III. Contract AF 04(647)-942

UNCLASSIFIED